Experimental and numerical behavior of anisotropic laminated FRP thin-walled web beams under different loading and boundary parameters

by

Garima Sharma

B.E., Tribhuvan University, Nepal, 2018

A THESIS

submitted in partial fulfillment of the requirements for the degree

MASTER OF SCIENCE

Department of Civil Engineering
Carl R. Ice College of Engineering

KANSAS STATE UNIVERSITY
Manhattan, Kansas

2022

Approved by:

Major Professor

Dr. Hayder Rasheed

ABSTRACT

Structural elements made of fibrous composites are increasingly used in aerospace, automotive, civil and marine engineering applications due to their high stiffness and strength-to-weight ratio and corrosion resistance properties. Most of the composite structural elements are thin-walled and their design is often controlled by stability considerations mainly due to slenderness effects. Hence, for thin-walled slender composite beams, lateral torsional buckling (LTB) is the dominant failure mode regardless of the fiber orientations.

In this study, combined numerical and experimental investigations for lateral torsional buckling of laminated composite web-cantilever and simply support beams are presented. A total of twelve carbon-fiber beams with six different anisotropic layups having a nominal length to height (l/h) ratio of 10 and four glass-fiber reinforced polymer beams with varying l/h ratios were experimentally tested for cantilever and simply support conditions respectively. The experimental response is compared against a non-linear numerical solution using Static Riks Analysis (SRA) to compare the predicted vs. actual load-displacement curve. An analytical approach, developed in an earlier study, was used to find the critical buckling load. Eigen value analysis was performed to benchmark the analytical buckling load using Abaqus.

ACKNOWLEDGEMENTS

I would like to express my deepest gratitude for the continuous support and guidance of my major advisor, Dr. Hayder A. Rasheed, whose insight and knowledge into the subject matter steered me through this research. I would also like to thank Head of Department, Dr A S M Hossain, who gave me a chance to be a part of this university.

I would also like to thank Dr. David Rosowsky and Dr. Krishna Ghimire for their willingness to serve on my supervisory committee.

I would like to specially thank my parents Bhanu Bhakt Sharma and Puspa Gautam, my esteemed sisters Madhuri Sharma and Priyanka Sharma, for their love and care, sacrifices, commitment to my education, and continuous prayers. Although your physical presence was heavily missed in this journey, but the inspiration and support provided me with much strength. Also, my deepest gratitude to my friends who made this journey much easier and get through some of the hardest times.

Finally, I would like to thank my master Sri Ravi Shankar who have inspired me to fulfill my duties and commitment and helped in moving forward in life.

Contents

LIST OF FIGURES

LIST OF TABLES

CHAPTER 1 : INTRODUCTION

1.1 Overview/ Background:

The use of traditional construction materials like steel, concrete and timber are very prevalent in structural applications. In recent years, the degradation of concrete, steel and timber materials in various structures has become increasingly evident, affecting the normal use and service life of these structures and introducing significant safety hazards (Hu et al., 2020). To effectively address this important issue, researchers have shown interest in advanced fiber-reinforced polymer composite materials.

Composites such as Fiber Reinforced Polymers (FRP) are made up of two or more materials with different physical and chemical properties. Fiber and matrix are the two main components of FRP composites. The fibers provide structural strength and stiffness in their direction of application while the matrix is responsible of holding the fibers together and transferring the load among them. Furthermore, the mechanical properties of the composite are entirely determined by the properties of the fiber and the quality of the fiber/matrix interface. (Hollaway 2010)

The use of FRP can be dated back to 1950s, in the aerospace industry, with its application in structural elements like horizontal and vertical stabilizers, flaps, wings and various control surfaces. The popularity of FRP in the industry can be attributed to its high strength to weight ratio, high stiffness to weight ratio and corrosion resistance. According to Hariz et al. (2021), a composite technology approach can result in a significant reduction in tailored structural material. Vertical and horizontal stabilizers, wing skins, and flaps, for example, are made of advanced composites in fighter aircraft, resulting in weight savings of up to 20%.

Although FRP has superior characteristics to other materials, their widespread use in the industry is somewhat limited. This may be attributed to the fact that the design formulas and guidelines developed for homogenized isotropic materials cannot be directly applied to FRP due to their complex laminated architecture. (Halim 2020)

Because of the impacts of their slenderness, thin-walled member designs are frequently governed by stability considerations. Consequently, lateral torsional buckling is the predominant failure mode for thin-walled composite beams. This failure mechanism known as lateral-torsional buckling (LTB) is defined by the lateral bending coupled with twisting of the cross section that is originally bent by its strong axis. LTB is primarily controlled by the geometric slenderness ratio combined with the complex material response.

The lateral-torsional buckling may include two distinct behavior features: elastic and inelastic. Members with low slenderness ratio experience inelastic lateral-torsional buckling whereas members with high slenderness ratio experience elastic lateral-torsional buckling. It is a topic of concern when dealing with members of high slenderness ratio as occurrence of LTB significantly reduces the load carrying capacity of the member.(Ahmadi 2017)

In a study conducted for LTB of cantilever beams by Rasheed et.al. (2020), an analytical formulation was developed to find the critical load of carbon FRP web beams with varying L/h ratios and different stacking sequences. The critical load calculated was independent of the ultimate strength and was governed by the geometry and material laminations of the member. Similar analytical formulation was developed by Ahmadi and Rasheed (2018) for simply supported condition for composite beams with anisotropic layups subjected to mid-span concentrated load.

This study extends the recent research work to verify the analytical solutions developed for the lateral torsional buckling of cantilever and simply supported beams by experimental testing and evaluation as well as numerical simulations using the finite element methods.

1.2 Objectives:

The main objectives of this study are:

- To verify the analytical model developed earlier against numerical and experimental results for lateral-torsional buckling of anisotropic laminated cantilever Carbon Fiber Reinforced Polymer (CFRP) web beams.
- To validate the analytical model developed earlier against numerical and experimental results for lateral-torsional buckling of anisotropic laminated Glass Fiber Reinforced Polymer (GFRP) web beams in a simply supported boundary condition.

1.3 Scope:

The style of this thesis is formatted around the collection of two journal papers. The thesis includes a total of five chapters describing the lateral-torsional buckling of anisotropic beams under varying loading and support conditions using carbon and glass FRP. The first chapter presents brief overview, objectives and scope of the thesis. The second chapter includes the literature review undertaken on the topics related to the thesis scope. Chapter three is devoted to the first journal paper about the stability analysis of anisotropic laminated web cantilever beams under tip force. Chapter four introduces the work conducted on GFRP simply supported web beams subjected to mid- height force at the midspan, which comprises the second paper. This chapter further validates the experimental results with the numerical solution using finite element analysis. Chapter five summarizes the work done in the research with the outcomes, conclusions and conclusions and possible future work.

CHAPTER 2 : LITERATURE REVIEW

The design of thin walled beams is mainly governed by its stability which in turn depends on its slenderness effect. Several studies have been done before to the understand the buckling of beams.

Many comparative studies have been done for the Lateral torsional buckling of beams. Bank et al. investigated the theoretical and experimental evaluation of local compression flange buckling in pultruded fiber -reinforced plastic I beam. Four-point testing was conducted in the study to record the buckling load and stresses using strain gages and LVDTs. In addition to the measured buckling loads and stresses, their predicted theoretical measurements were reported. Upon comparison, it was concluded that the theoretical model correctly estimated the edge rotational restraint coefficient and the corresponding buckling stress. (Bank et al. 1994)

Davalos et al. proposed an analytical formulation for lateral torsional buckling of wide flange beams that was validated using experimental and numerical data. The analytical equation was developed using energy principles and nonlinear elastic theory. Two wide flange beams were tested under midspan concentrated loading for the experimental setup. The study concludes that the numerical, analytical, and experimental results are all in good agreement. (Davalos et al. 1997)

A similar comparative study was conducted for I beams,(Davalos et al. 1997) , and open channel beams, (Shan and Qiao 2005). In the first study, two I-beams were tested under midspan loading to validate the analytical expression. The analysis was based on energy principles and non-linear elastic theory was used to derive the total potential energy equations for the instability encountered in FRP I beams. The total potential energy in the equilibrium equation was solved by the Rayleigh-Ritz method to formulate a simplified equation. Finally, comparing the experimental

results with those obtained from the numerical evaluation indicated that the formulated analytical design equation could be adopted to predict the loading for flexural torsional buckling.

Thumrongvut and Seangatith experimentally tested 26 pultruded fiber reinforced plastic (PFRP) cantilever channel beams to verify the effect of the unbraced length on the lateral torsional buckling. The critical buckling moment calculated by the modified LRFD steel design equation was compared with the obtained buckling moments from this experiment. The results were in good agreement when the span to depth ratio was greater than 10, however, the predicted results were on the conservative side for span to depth ratio less than 10. (Thumrongvut and Seangatith 2011)

A two part study was conducted by Correia et al. to examine the buckling and post-buckling behavior of GFRP pultruded I beams. Its first part was a full-scale experimental study where beams were tested in cantilever and simply supported condition. Their mechanical properties were assessed by tensile, interlaminar shear, flexural and compressive tests. Full-scale testing indicated several differences in the structural behavior of beams made of traditional materials. The failure mechanisms triggered by local and global lateral torsional buckling were clearly demonstrated in the results for simply supported and cantilever beams. (Correia et al. 2011)

Its second part was based on the numerical simulations given by Silva et.al. for the structural response of simply supported and cantilever beams. The results assessed were in accordance with (i) the experimental results reported in the first part, and (ii) the analytical measurements documented in the literature. (Silva et al. 2011)

(Laudiero et al.) simulated a numerical approach for the buckling resistance of pultruded FRP profiles under pure compression and uniform bending in two parts. The first section used non-linear finite element analysis to determine the buckling mode interaction in wide flange columns under pure compression while accounting for imperfections. The numerical results indicated that the imperfection amplitude played a crucial role making the columns unsafe. In the second part, a

similar approach was used for beams with uniform bending. Finally, an expression for the rotational spring stiffness of the web-flange junction was proposed, yielding more accurate results for local buckling. (Laudiero et al. 2012)

An experimental and numerical study on the lateral torsional buckling of steel I beams retrofitted with bonded and unbonded CFRP laminates with varying pre-stress levels by Ghafoori and Motavalli. A total of seven beams were tested until failure. Although the time required to prepare the bonded beam was twice that of the unbonded beam, the increase in elastic stiffness was equivalent for both beams. The reduction in stress at the beam bottom flange was a slightly higher advantage of using the bonded beam. Furthermore, the prestressing had no effect on elastic stiffness but had a significant effect on buckling strength. It can be inferred that to strengthen metallic beams with prestressing laminates, bonded FRP would be an effective solution. (Ghafoori and Motavalli 2015).

Prachasaree et al. proposed a simplified buckling strength equation for lateral torsional buckling and local buckling strengths of FRPs structural members. The proposed equation was compared to a prestandard equation and experimental data gathered from previous researchers' works. When compared to experimental data, the results for lateral torsional buckling were conservative. Furthermore, when compared to buckling strength based on prestandard equations, LTB was directly proportional to its unbraced length. The proposed equation demonstrated 15% average percentage difference with the experimental data for local buckling strength. The authors suggest that that results were accurate and reliable for easier calculations. (Prachasaree et al. 2019)

Based on the second variational principle and nonlinear plate theory, an analytical formulation for channel beams was developed. Three beams with different geometries were tested in cantilever configuration for the experimental setup. The experimental findings were validated

using numerical runs. The comparable results between the three approaches, analytical, numerical, and experimental, suggest that the analytical formulation could be used in future work.

Zeinali et. al. performed experimental-numerical study on lateral torsional buckling of pultruded FRP I-section beams having different span to height ratios under pure bending. Using Eurocode 3 provisions, reasonable agreement between experimental and numerical results has been reported. (Zeinali et al. 2020)

The number of studies performed on the lateral torsional buckling shows that the failure mode by this phenomenon is a serious concern and should be brought to specific attention. The study herein investigates the LTB on cantilever and simply supported condition for anisotropic laminated Carbon FRPs and Glass FRPs by numerical and experimental testing to examine the most general fiber architecture.

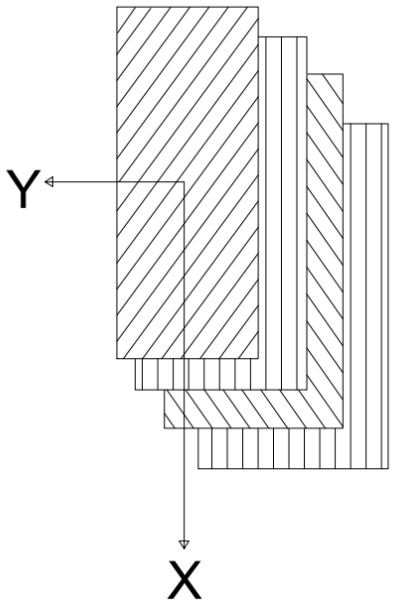

Fig 2. 1 Typical stacking sequence

REFERENCES

Ahmadi, H. 2017. “Lateral Torsional Buckling of Anisotropic Laminated Composite Beams Subjected to Various Loading and Boundary Conditions.” *ProQuest Diss. Theses*. Ph.D. Ann Arbor: Kansas State University.

Bank, L. C., M. Nadipelli, T. R. Gentry, and J. S. Yin. 1994. “Local Buckling of Pultruded FRP Beams: Theory and Experiment.” 417–422. ASCE.

Correia, J. R., F. A. Branco, N. M. F. Silva, D. Camotim, and N. Silvestre. 2011. “First-order, buckling and post-buckling behaviour of GFRP pultruded beams. Part 1: Experimental study.” *Comput. Struct.*, Civil-Comp, 89 (21): 2052–2064. https://doi.org/10.1016/j.compstruc.2011.07.005.

Davalos, J. F., P. Qiao, and H. A. Salim. 1997. “Flexural-torsional buckling of pultruded fiber reinforced plastic composite I-beams: experimental and analytical evaluations.” *Compos. Struct.*, Ninth International Conference on Composite Structures, 38 (1): 241–250. https://doi.org/10.1016/S0263-8223(97)00059-7.

Ghafoori, E., and M. Motavalli. 2015. “Lateral-torsional buckling of steel I-beams retrofitted by bonded and un-bonded CFRP laminates with different pre-stress levels: Experimental and numerical study.” *Constr. Build. Mater.*, 76: 194–206. https://doi.org/10.1016/j.conbuildmat.2014.11.070.

Halim, A. H. 2020. “Lateral Torsional Buckling of Thin-Walled Rectangular and I-Section Laminated Composite Beams with Arbitrary Layups.” *ProQuest Diss. Theses*. Ph.D. Ann Arbor: Kansas State University.

Hollaway, L. C. 2010. “A review of the present and future utilisation of FRP composites in the civil infrastructure with reference to their important in-service properties.” *Constr. Build. Mater.*, Special Issue on Fracture, Acoustic Emission and NDE in Concrete (KIFA-5), 24 (12): 2419–2445. https://doi.org/10.1016/j.conbuildmat.2010.04.062.

Laudiero, F., F. Minghini, N. Ponara, and N. Tullini. n.d. “BUCKLING RESISTANCE OF PULTRUDED FRP PROFILES UNDER PURE COMPRESSION OR UNIFORM BENDING□NUMERICAL SIMULATION.” 8.

Prachasaree, W., S. Limkatanyu, W. Kaewjuea, and H. V. GangaRao. 2019. “Simplified buckling-strength determination of pultruded FRP structural beams.” *Pract. Period. Struct. Des. Constr.*, 24 (2): 04018036. American Society of Civil Engineers.

Shan, L., and P. Qiao. 2005. “Flexural–torsional buckling of fiber-reinforced plastic composite open channel beams.” *Compos. Struct.*, 68 (2): 211–224. https://doi.org/10.1016/j.compstruct.2004.03.015.

Silva, N. M. F., D. Camotim, N. Silvestre, J. R. Correia, and F. A. Branco. 2011. “First-order, buckling and post-buckling behaviour of GFRP pultruded beams. Part 2: Numerical simulation.” *Comput. Struct.*, Civil-Comp, 89 (21): 2065–2078. https://doi.org/10.1016/j.compstruc.2011.07.006.

Thumrongvut, J., and S. Seangatith. 2011. “Experimental Study on Lateral-Torsional Buckling of PFRP Cantilevered Channel Beams.” *Procedia Eng.*, The Proceedings of the Twelfth East Asia-Pacific Conference on Structural Engineering and Construction, 14: 2438–2445. https://doi.org/10.1016/j.proeng.2011.07.306.

Zeinali, E., A. Nazari, and H. Showkati. 2020. “Experimental-numerical study on lateral-torsional buckling of PFRP beams under pure bending.” *Compos. Struct.*, 237: 111925. https://doi.org/10.1016/j.compstruct.2020.111925.

CHAPTER 3 : PAPER 1

Stability Analysis of Anisotropic Laminated Web-Cantilever Beams Under Tip Force: Experiments vs. Predictions

Garima Sharma[1], Fahed H. Salahat[2] and Hayder A. Rasheed[3]

[1]M.Sc. Student, Department of Civil Engineering, Kansas State University, Manhattan, KS (garimas@ksu.edu)

[2]Ph.D. Student Department of Civil Engineering, Kansas State University, Manhattan, KS (salahatf@ksu.edu)

[3]Professor, Department of Civil Engineering, Kansas State University, Manhattan, KS (hayder@ksu.edu)
Corresponding author

3.1 ABSTRACT

A combined numerical and experimental study for lateral torsional buckling of laminated composite web-cantilever beams is presented. A total of twelve beams with six different anisotropic layups were prepared using wet/hand layup method having a nominal length to height (l/h) ratio of 10. The beams were manually loaded in small increments and the point of load application was located at the mid height of its free end. Two laser dots were mounted horizontally at the top and bottom of the free end to project laser lights that help trace the angle of twist at each load increment. This technique was used to trace the angle of twist associated with each load level during testing. The experimental response is compared against a non-linear numerical solution using Static Riks Analysis (SRA) to generate the predicted load-displacement curve. It is evident that the two curves generally compare well when initial imperfections are numerically accounted for. An analytical approach, developed in an earlier study, was used to find the critical buckling load. Eigen value analysis was performed to benchmark the analytical buckling load using Abaqus. Overall, the limit loads from the numerical, experimental and analytical solutions appear to be in good agreement.

3.2 INTRODUCTION

Fiber Reinforced Polymers (FRP) are manufactured by combining dry fiber fabrics with polymetric resin matrix at a macroscopic level. In comparison to other conventional materials like concrete and steel, the use of FRP in engineering applications is relatively new. Because of their lightweight and design versatility, Fiber Reinforced Polymer (FRP) composites are expanding their way into many engineering disciplines especially the aerospace industry. Due to their superior characteristics, FRPs are paving their path in the civil engineering industry as well.

Plates, bars and different thin-walled open and closed section structural shapes made of FRP are now produced by various manufacturers. An important limit state encountered when designing such elements is often controlled by stability (buckling) considerations due to slenderness effects. Many studies considered the development of analytical models to predict the failure of slender sections subjected to multitude of stress states, e.g. bending, shear and torsion. A major failure mode identified is the lateral torsional buckling. It is a phenomenon in which beams buckle due to combined effect of twisting and lateral bending when subjected to loading about the strong axis.

Davalos and Qiao (1997) considered the flexural-torsional buckling of FRP wide-flange beams through combined analytical and experimental studies. An analytical model was derived based on non-linear elastic theory to predict the total potential energy required to cause instability of the wide-flange beams subjected to midspan concentrated loads. The model was validated against experimental testing of two geometrically identical FRP wide-flange beams and the results showed good agreement in predicting the flexural-torsional buckling loads.

Lee and Kim (2002) studied the flexural-torsional coupled vibration of thin-walled composite beams with channel sections. A proposed model was developed based on classical lamination theory to account for the coupling of flexural and torsional effects of arbitrary

laminate stacking sequence configuration. The results were found to be appropriate and efficient in analyzing free vibration problem of thin walled laminated composite beams.

Qiao et al. (2003) developed simple equations to determine the flexural-torsional buckling of I-beams loaded at the centroid of the tip cross-sections. The equations were derived using the nonlinear plate theory including the shear effect and bending-twisting coupling. Experimental and numerical studies were also done to verify the analytical solution. The results confirmed the accuracy of the proposed equations in predicting the flexural-torsional buckling load of I-beams.

Vo and Lee (2007) studied the flexural-torsional behavior of thin-walled closed-section composite box beams using an analytical model based on classical lamination theory. The model accounts for the coupling of flexural and torsional response of the box section considering the effect of varying the fiber's orientation angle and the laminate stacking sequence configuration.

Kim et al. (2007) evaluated the exact element stiffness matrix to perform flexural-torsional stability analysis of thin walled composite beams with symmetric and arbitrary stacking sequence configuration subjected to a compressive force. The proposed method can be used as a general solution to obtain the flexural-torsional buckling load for any boundary condition. The proposed model showed good agreement when compared against numerical simulations.

Ascione et al. (2011) presented a mechanical model capable of considering the contribution of shear deformation on the lateral buckling behavior of open-cross sections pultruded FRP beams. The proposed model considered the approximation of shear strains which are neglected by classical Vlasov theory. The results obtained by applying this model were validated against numerical results from the literature and showed that the effect of shear strains led to reducing the buckling load for the considered sections.

Rasheed et al. (2017) developed analytical approach for lateral-torsional buckling of simply supported anisotropic steel-FRP beams under pure bending condition using the classical laminated theory. The results were favorably benchmarked against Eigenvalue and nonlinear geometry finite element analysis using Abaqus. Based on the study, it has been shown that stability of beams under pure bending is greatly affected by the length to height (l/h) ratio and the laminate stacking sequence configuration.

Rasheed et al. (2020) extended their analytical approach to obtain semi-analytical closed form buckling formula for rectangular anisotropic laminated cantilever beams subjected to tip force. The results of this formula were in close agreement with numerical results from Abaqus for a wide range of lamination stacking sequences. This formula is used in the present study to benchmark the experimental and numerical results generated herein.

In a study by Kasiviswanathan and Anbarasu (2021), a simplified approach was presented to find the lateral torsional buckling of GFRP channel beams. The study provides an equation for the safe design strength. The channel beams were tested in simply supported configuration subjected to uniform bending about their major axis. Abaqus was used for the finite element of the beams with varying sectional geometry and span of beam. The FE model was verified using the results provided in the literature. The numerical model was verified against the theoretical values provided in Eurocode 3 of steel sections revealing discrepancies in the results.

Anbarasu and Kasiviswanathan (2021) developed a simplified design formulation to find the lateral torsional buckling of pultruded GFRP I beams. Abaqus was used for the finite element simulations of the model in simply supported condition. The FE model was verified using the relevant data provided in the literature of the study. The strength obtained from the numerical

runs were assessed with the theoretical LTB strength predicted by the equations proposed for the GFRP beams available. The results were over-conservative esp. in the low and medium slenderness range.

A research team of EL-Fiky et al. (2022)covered 70 works about recent activities and future implementation on FRP fiber poles. The study considered six major aspects: introduction, methodology, material properties, manufacturing technique, testing and modeling of FRP poles. For manufacturing, the team concluded that the most suitable method was centrifugal process. Because of qualities like UV resistance and energy absorption, glass fiber was considered to be the best choice for FRP poles. Furthermore, the results from FE model and experimental results were very similar.

In this study, lateral torsional buckling of generally anisotropic rectangular or web beams is examined as a first step in addressing web-stiffened horizontal panels which are common in aerospace and off-shore structures. The reason this beam configuration is called web beam is the fact that the structural system is envisioned to be composed of several parallel webs attached to a common flat plate (i.e. stiffened horizontal plate). Therefore, thin web-cantilever beams made of Carbon FRP are designed, fabricated and tested to generate experimental response curves. These curves are compared against Eigenvalue and nonlinear finite element simulations using Abaqus. Furthermore, they were also compared against the results of the analytical formula derived by Rasheed et al. The results appear to be in good agreements for a variety of anisotropic stacking sequences utilized.

3.3 ASSUMPTIONS

The following assumptions are made in the analytical treatment established earlier:

1) The material is generally anisotropic laminated composite with elastic properties using thin plate classical lamination theory.
2) The kinematics assumes twisting angle to be constant across the height of the beam.
3) The strain-displacement relationship is assumed to be linear.
4) The equilibrium equation is linearized for buckling analysis.
5) The non-linear terms from the loading are retained in the governing differential equation.

The following assumptions are made in the numerical treatment addressed here:

1) The material is generally anisotropic laminated composite with elastic properties using moderately thick shell elements.
2) The kinematics captures the actual variation of the twisting angle across the height of the beam.
3) The strain-displacement relationships are assumed to be non-linear within Riks Analysis.
4) The equilibrium equations are linearized for Eigen Value Analysis while they are fully non-linear within Riks Analysis.
5) The imperfections are treated using notional loads.

Assumption 1 is proven to be accurate experimentally since the beam goes to its original undeformed configuration after load removal indicating no induced damage.

3.4 COMPOSITE BEAM FABRICATION PROCESS

The beams were prepared in the composite lab at Kansas State University using wet/hand layup method. Four laminas of CFRP (V Wrap C100 2022) were applied to fabricate each beam. Epoxy resin (V-Wrap 770 2022) was used to saturate all layers of the laminates. Since, the carbon fiber fabric is unidirectional, the sheets were cut in a manner shown in **Fig 3. 1** to get the desired fiber angles for the designated stacking sequences.

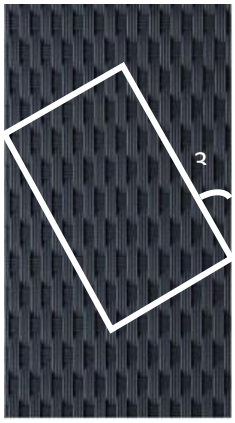

Fig 3. 1 . Layout for obtaining 30º orientation from unidirectional fabric

Once the dry fiber fabric was cut to the specific angles targeted, the fabric strips were laid on wax paper while a coat of epoxy was used to evenly saturate all four layers. After impregnating the fibers with resin, the beams were left to cure for 7 days at room temperature, see **Fig 3. 2** . Once the curing process is concluded, the beams were cut to their specified dimensions, see **Table 3. 1**, leaving an extension along the beam length to properly grip the beam at the fixed end. The beam dimensions were measured using a digital caliper whereby three measurements were made for the width and thickness which were averaged out for the purpose of numerical analysis. On the other hand, the length of each beam was measured with a measuring tape and was recorded as given in **Table 3. 1**.

Fig 3. 2. Beams left for curing after fabrication

Table 3. 1. Beam Designations and Dimensions

Layup ID	Dimension (mm) Length x Height	Thickness(mm)	Layup sequence
1	485 x 51.1	2.872	30/-30/30/-30
1	245 x 25.4	2.049	30/-30/30/-30
2	500 x50	2.796	30/30/30/30
2	250 x 25	2.688	30/30/30/30
3	500 x50	2.712	30/-30/-30/30
3	250 x 25	2.668	30/-30/-30/30
4	500 x50	2.648	15/0/-15/30
4	250 x 25	2.804	15/0/-15/30
5	500 x50	2.720	15/30/-45/15
5	250 x 25	2.700	15/30/-45/15
6	500 x50	2.716	30/-30/45/-45
6	250 x 25	2.656	30/-30/45/-45

3.5 MATERIAL CHARACTERIZATION

The carbon fiber used to manufacture the present composite beams is V-Wrap C-100 having the mechanical properties given in **Table 3. 2**. A two-component epoxy resin named V-wrap 770, **Table 3. 2**, was used to saturate the fiber by following the wet layup manufacturing process. By using the properties of the dry fiber and the resin as well as the principles of composite micromechanics, the cured laminate properties were computed as per Rasheed (2014). A sample of these calculations is shown in **Appendix A** and the results are listed in **Table 3. 3**.

Table 3. 2. V-Wrap C-100 fiber (dry) and V-Wrap 770 epoxy resin mechanical properties

Property	Value
V-Wrap C-100	
Primary fiber direction	0 degree (unidirectional)
Weight per square yard	300 g/m^2
Tensile strength	4,480 MPa
Tensile modulus	234,400 MPa
Thickness	0.165 mm
Elongation	1.9%
Poisson's ratio	0.4
V-Wrap 770 Epoxy adhesive	
Flexural Modulus	2,620 MPa
Poisson's ratio	0.0315

Table 3. 3. Cured laminate properties recovered from micromechanics relationships.

Layup ID	Dimensions (mm)	E_1 (MPa)	E_2 (MPa)	v_{12}	G_{12} (MPa)	G_{23} (MPa)
1	485 x 51.1	55960.40	4202.36	0.324	1535.94	1533.78
1	245 x 25.4	57874.19	4330.26	0.322	1557.12	1580.39
2	500 x 50	56532.50	4245.14	0.323	1526.94	1549.32
2	250 x 25	58781.99	4388.59	0.322	1577.79	1601.67
3	500 x 50	58289.56	4356.88	0.321	1566.55	1590.10
3	250 x 25	59210.92	4416.35	0.322	1587.63	1611.81
4	500 x 50	59646.34	4444.67	0.320	1597.66	1622.14
4	250 x 25	56401.84	4236.91	0.322	1524.02	1546.32
5	500 x 50	58081.11	4343.51	0.321	1561.81	1585.22
5	250 x 25	58499.56	4370.38	0.321	1571.34	1595.03
6	500 x 50	58185.14	4350.17	0.321	1564.18	1587.66
6	250 x 25	59464.12	4432.80	0.320	1593.46	1617.81

3.6 EXPERIMENTAL SETUP

All beams were tested in cantilever configuration and the tip force loading was applied at the mid height section of the beam. To capture the tip deformation of the cantilever beam, a frame made out of PVC pipes was built with plexi-glass screen on which Engineering Paper was attached to trace the progression of deformation, see **Fig 3.3.**.For the cantilever configuration to be achieved, one end of the beam was clamped to a mechanical vise, see **Fig 3. 4**. To track the deformation of the tip end of the beam, two laser dots were mounted at the top and bottom of the

tip section of the cantilever beam, see **Fig 3. 5**. By drawing a line on the Engineering Paper connecting the reflection of the two laser dots, the deformation path of the beam tip section is traced at each load step, see **Fig 3. 4-Fig 3. 6**. To load the beam at the free end, a small hole was drilled at the cantilever tip, in which an annular steel bush was inserted to avoid damaging the composite material by the load application, see **Fig 3. 5**. A nylon string was passed through the hole and tied to the two ends of a metal rod to allow the load to be aligned with the loading hole during deformation, see **Fig 3. 7**. The load is applied by adding lead shots into a small bucket that is connected to the center of the horizontal rod, see **Fig 3. 7**. To get the points for the angle of twist, the reflection of the two laser dots on the engineering paper is connected by colored pens that are uniquely associated with each loading step, see **Fig 3. 7**. Upon conclusion of the experiment, the engineering paper is removed and digitally scanned using a software called digitizeit to extract the load vs angle of twist data.

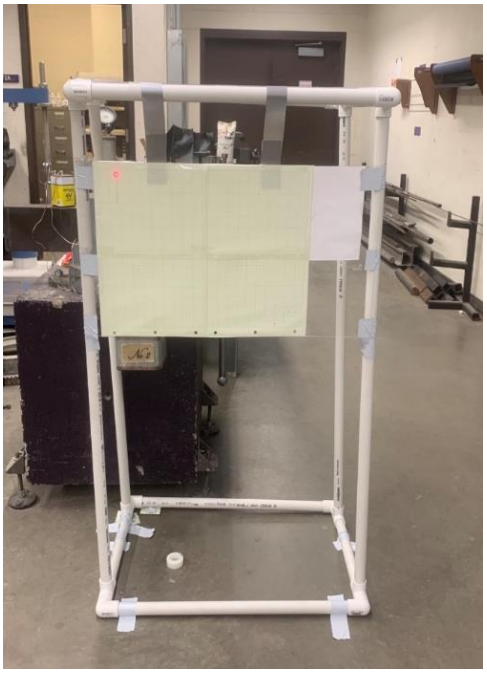

Fig 3. 3. Front view of the experimental

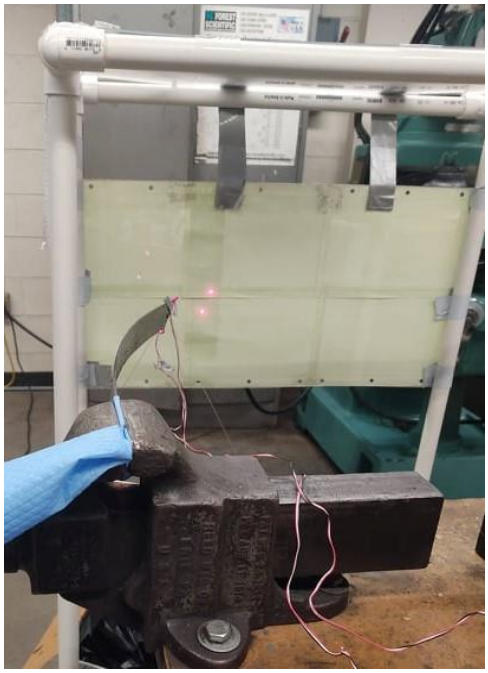

Fig 3. 4. Beam in buckled configuration

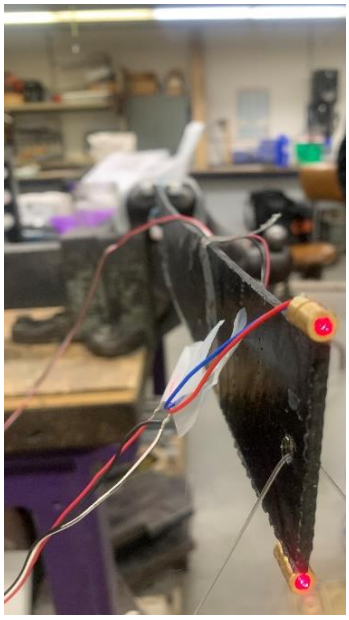

Fig 3. 5. Mounting laser dots for tracing the angle of twist.

Fig 3. 6. Beam in buckling configuration with laser dots reflected on the tracing screen.

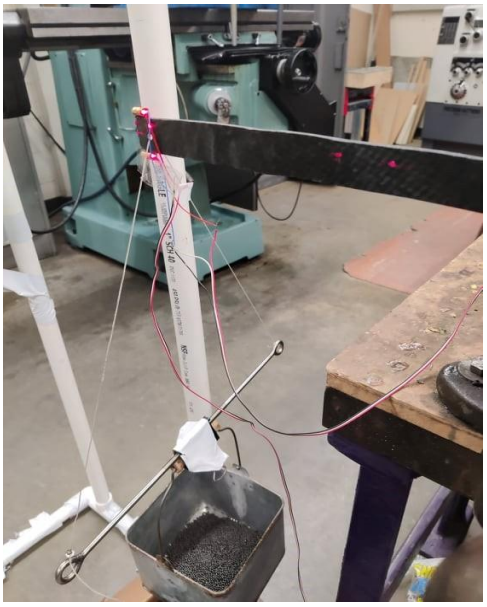

Fig 3. 7. Nylon string used to hold loading bucket

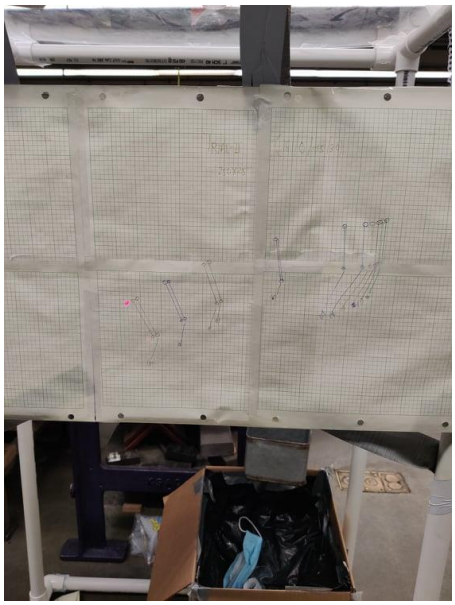

Fig 3. 8. Laser light being projected for the deformation lines

3.7 NUMERICAL ANALYSIS

Numerical analysis was performed by implementing two independent techniques using the multi-physics software Abaqus. The first technique uses Eigen Value Analysis (EVA) to establish the anticipated buckling load while the second technique uses full non-linear finite element Static Riks Analysis (SRA). Details of these two techniques are given below:

3.7.1 Eigen Value analysis (EVA)

Mechanical properties of the cured laminates along with their fiber orientation were input into the software. The beams in the model were created using 3D planar shell elements. After the beam with its proper dimensions was generated, the stacking sequence was input in the software using the composite layup. Following the composite layup process, the material properties were assigned to the beam. A specific load was applied at the mid-height of the beam at the free end. Before the analysis, the beam was meshed with standard quadratic quadrilateral shell element type of S8R (8- node doubly curved thick shell element with reduced integration) with a mesh size of 5mm along the beam axis, see **3.10.(a)**. The value obtained from Abaqus for the first mode was

multiplied by the applied load amount to get the actual buckling load. For the EVA, the software uses the Lanczos solver which reduces an m x m symmetric matrix using recurrence relations to a tridiagonal matrix (Hernandez et al. 2006).

3.7.2 Static Riks Analysis (SRA)

This method uses arc length technique to capture the full non-linear response of beams. Memon and Su (2004) addressed the limitations in tracking the load-displacement curve by standard load-controlled or displacement-controlled solutions which can be avoided using the arc length method. In the arc length method, a portion of load is initially applied as a load step to determine load-displacement values for normalizing subsequent steps.

The buckling load obtained from the Eigen value analysis was used to define the target load which is used by the arc length solver to determine the intermediate load steps based on defined increments. Different notional loads were applied to produce an equivalent initial imperfection in the angle of twist. These notional loads are defined as small percentages of the actual applied vertical tip force. The direction of the notional loads was determined by the buckling behavior observed in EVA as shown in **Fig 3. 9**.

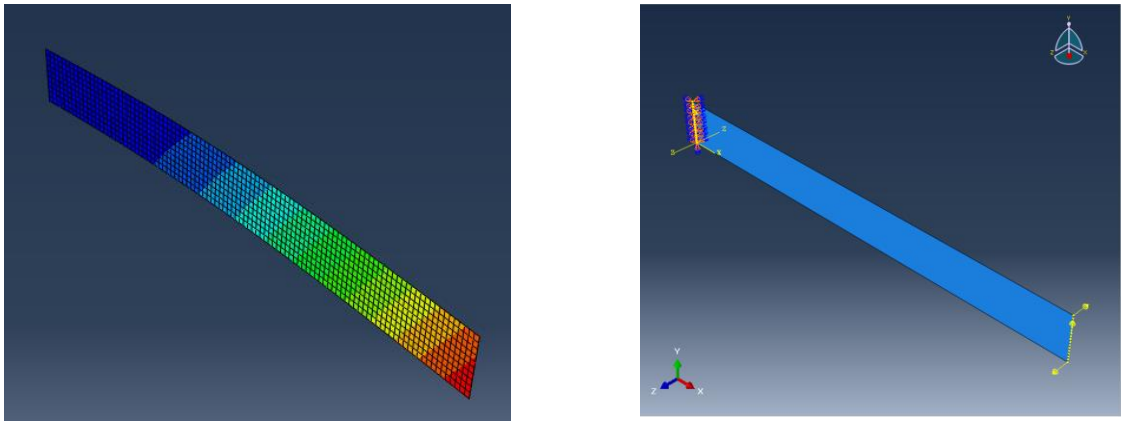

(a) (b)

Fig 3. 9. Notional load assignment (a) buckled shape (b) applied imperfection

3.8 ANALYTICAL FORMULATION

Analytical Predictions were made using a solution developed by Rasheed et al. (2020) based on classical lamination theory embedded into Vlasov plate formulation. A closed form solution was obtained by extending the dimensional reduction to 3D constitutive matrix. Following a two-step process, first the shear strain, lateral curvature and twisting curvature were recovered by the static condensation technique. Effective lateral, torsional and coupling stiffness were retained by condensing the shear strain variable in the second step. To formulate the two differential equations in terms of lateral curvature and twisting angle, equilibrium conditions were applied in the deformed configuration. Finally, with the proper elimination of lateral curvature, the twisting angle differential equation having non-constant coefficients was generated. This equation was solved using a hybrid numerical-analytical approach yielding an analytical buckling expression. The entire analytical formulation was presented in detail in an earlier article by Rasheed et al. (2020). The critical buckling load can be calculated from the formula given below in Eq. (1).

$$P_{Cr} = \frac{C_2 h}{L^2}\sqrt{4[D_Y D_T - {D_{YT}}^2]} \qquad \text{Eq. (1)}$$

where $C_2 = 4.0038e^{-0.719C_1}$, $C_1 = |D_{YT}|/\sqrt{D_Y D_T - {D_{YT}}^2}$, D_Y is the effective lateral bending stiffness, D_T is the effective torsional stiffness and D_{YT} is the effective lateral torsional coupling stiffness.

3.9 RESULTS AND DISCUSSIONS

A group of cantilever web beams were designed, manufactured and tested in the composite lab at Kansas State University. Each beam was composed of 4 layers of CFRP having a nominal cured thickness of 0.584 mm per layer. The layup is composed of nominal length dimensions of 250 and 500 mm corresponding to nominal height dimensions of 25 and 50 mm, respectively,

maintaining an (l/h) ratio of 10 for both. The lamination orientation varied from 0º, 15º, 30º and 45º with various combinations thereof, see **Table 3. 4**.

Table 3. 4 also presents a comparison of the analytical prediction, Eigen value extraction and projected experimental buckling loads for all the beams constructed. It is evident from that table the analytical and numerical buckling loads have a very good correspondence. On the other hand, some of the experimental buckling loads may appear to be on the lower side by a certain margin, which doesn't indicate a discrepancy with numerical and analytical values. Rather, it represents the last recorded value in the experiment, which may not be precisely representing the final buckling load due to the laser projections going beyond the edge of the recording frame in these flexible beams, see **Fig 3. 4**

Table 3. 4. Analytical, numerical and apparent experimental buckling loads for all beams.

Layup ID	Dimension (mm)	Layup Sequence	Analytical buckling load (N)	Eigen value (N)	% Error	Maximum experimental load (N)
1	485 x 51.1	30/-30/30/-30	42.03	42.12	0.20	31.15
1	245 x 25.4	30/-30/30/-30	73.96	68.31	8.28	66.75
2	500 x 50	30/30/30/30	8.30	9.14	9.16	8.90
2	250 x 25	30/30/30/30	15.23	16.42	7.26	15.58
3	500 x 50	30/-30/-30/30	18.92	19.48	2.89	17.80
3	250 x 25	30/-30/-30/30	36.57	36.11	1.27	30.04
4	500 x 50	15/0/-15/30	13.87	14.90	6.93	15.02
4	250 x 25	15/0/-15/30	31.33	32.45	3.46	31.15
5	500 x 50	15/30/-45/15	13.27	15.02	11.63	15.49
5	250 x 25	15/30/-45/15	26.13	28.90	9.58	26.15
6	500 x 50	30/-30/45/-45	21.87	21.89	0.01	23.36
6	250 x 25	30/-30/45/-45	41.76	39.41	5.97	41.16

Fig 3. 10 presents the tip force-twisting angle response for all the tested beams listed in **Table 3. 4**, which will be discussed extensively below:

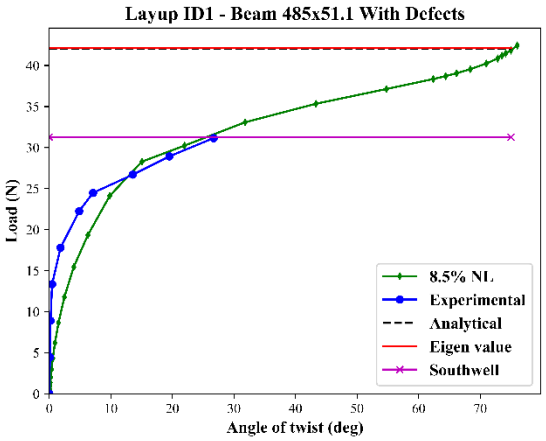

(a)

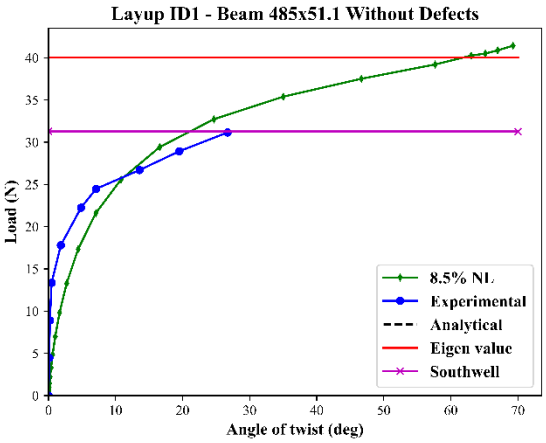

(b)

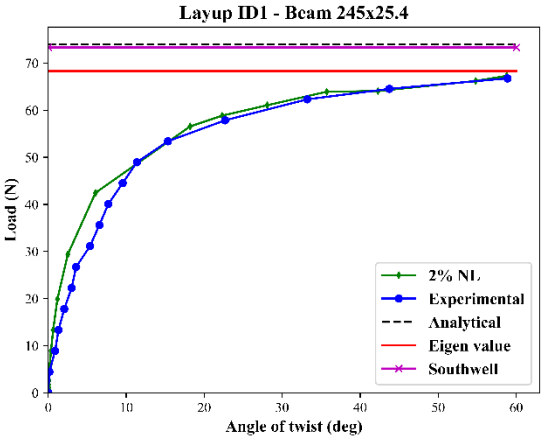

(c)

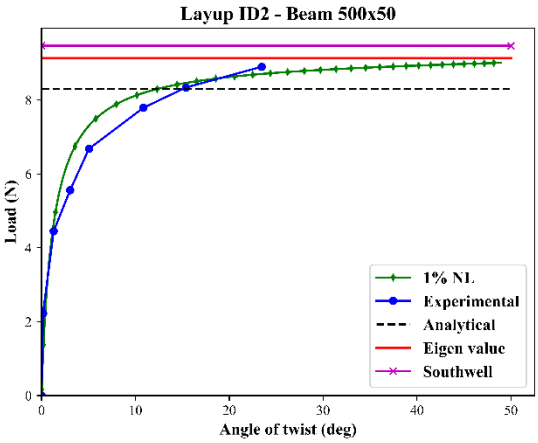

(d)

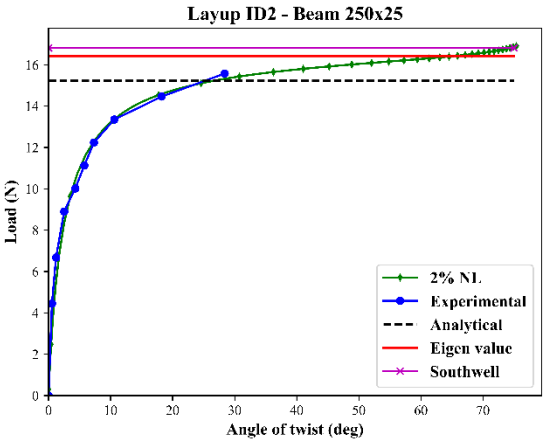

(e)

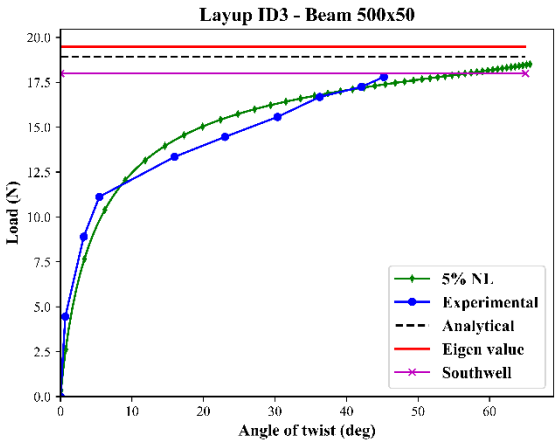
Layup ID3 - Beam 500x50
Load (N)
Angle of twist (deg)
5% NL
Experimental
Analytical
Eigen value
Southwell

(f)

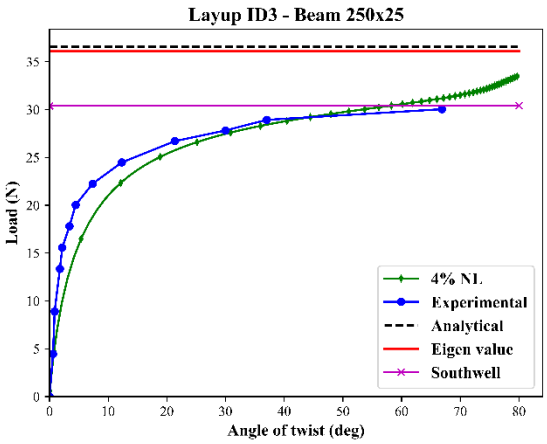
Layup ID3 - Beam 250x25
Load (N)
Angle of twist (deg)
4% NL
Experimental
Analytical
Eigen value
Southwell

(g)

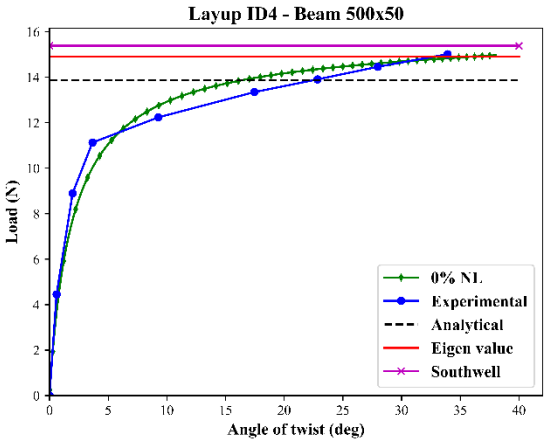
Layup ID4 - Beam 500x50
Load (N)
Angle of twist (deg)
0% NL
Experimental
Analytical
Eigen value
Southwell

(h)

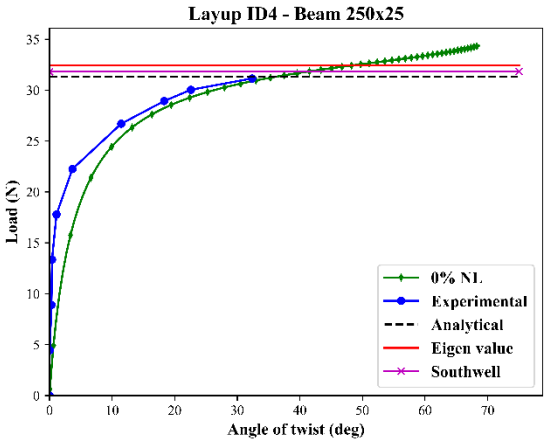
Layup ID4 - Beam 250x25
Load (N)
Angle of twist (deg)
0% NL
Experimental
Analytical
Eigen value
Southwell

(i)

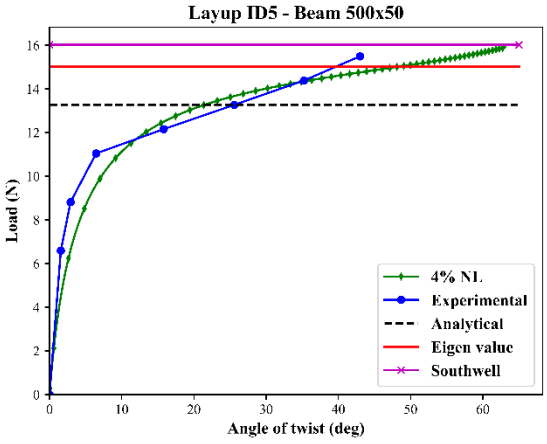
Layup ID5 - Beam 500x50
Load (N)
Angle of twist (deg)
4% NL
Experimental
Analytical
Eigen value
Southwell

(j)

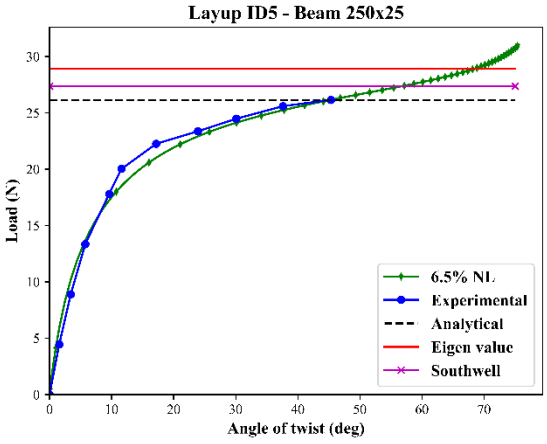
Layup ID5 - Beam 250x25
Load (N)
Angle of twist (deg)
6.5% NL
Experimental
Analytical
Eigen value
Southwell

(k)

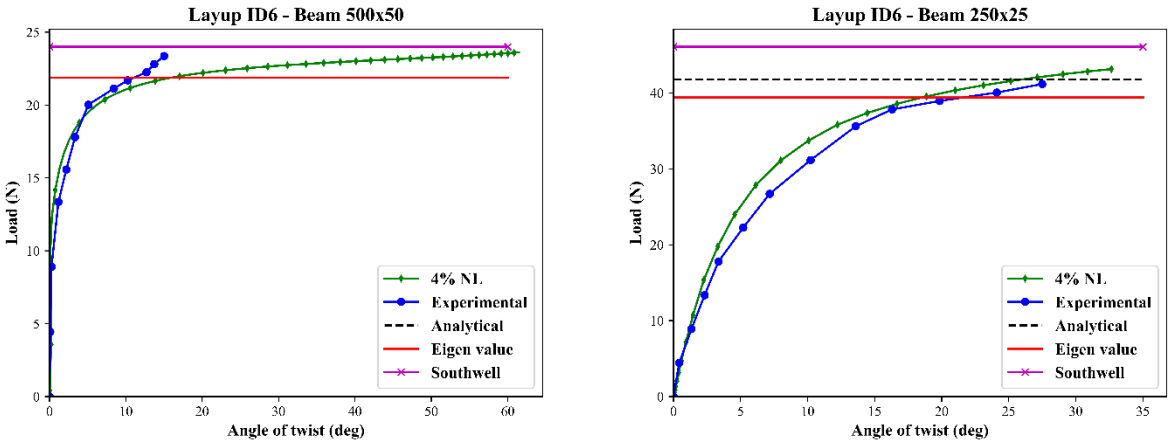

(l) (m)

Fig. 3. 10. Load Vs angle of twist examined for all beams tested

3.9.1 Layup ID 1

For the beam with balanced layup 30/-30/30/-30, there were two-member sizes having the same (l/h) ratio, see. The larger beam had a localized height defect in one of its layers. This was approximated by reducing the entire thickness of the defected layer in the analysis. For comparison purposes, two numerical runs were made for that beam with and without the accounting for the defect. The difference between the numerical and experimental curves may be attributed to the qualitative consideration of the defect. It can be seen from **Fig 3. 10** (a) that the analytical and eigen value results are matching almost perfectly (0.2% error). Furthermore, the non-linear response from the experimental and SRA is in good agreement up to the last recorded experimental load. It is evident that the effect of reducing the thickness of the defected layer has a minor effect on the results, as observed from **Fig. 3.** (a) and (b). Due to the lateral flexibility of this beam, the laser projections went off-limits of the framing screen sooner. Therefore, it was not possible to continue loading and collecting deformations beyond that point.

For the smaller beam, it is interesting to observe that the analytical and Eigen value results are somewhat off despite the fact the layup and the (l/h) ratio were the same as those of the larger beam. This may perhaps be attributed to the fact that **Eq. (1)** is seen to be a function of (l) and

(l/h) ratios. (Rasheed et al. 2020) study established this equation for different layups and (l/h) ratios under a constant (l) value of 500 mm. Therefore, this might have contributed to the discrepancy as compared to the EVA. On the other hand, the experimental curve and SRA response are seen to be in excellent agreement all the way to the buckling load, see **Fig 3. 10** (c).

3.9.2 Layup ID 2

For the anisotropic layup 30/30/30/30, the same large and small beams having a constant (l/h) ratio showed slight difference in the value in the critical buckling load obtained from the Analytical formula and EVA. However, the percentage error is very similar for both beam sizes.

For the non-linear response simulated from the SRA method, the experimental results for the larger beam were in excellent agreement with the numerical curve having 1% notional load. For the smaller beam, the experimental results matched exactly with the numerical approach using 2% notional load, see **Fig 3. 10** (d) and (e). It is interesting to observe that the highly anisotropic nature of this layup was accurately captured by the numerical analysis without discrepancies.

3.9.3 Layup ID 3

For the symmetric Layup ID 3 (30/-30/-30/30), the two beams, with same (l/h) ratio, showed relatively low levels of error between the analytical buckling load and the EVA. From **Table 3. 4**, it may be seen that the analytical buckling load of the smaller beam is slightly higher than the EVA load while the opposite is true for the larger beam.

It is evident that both beams show a reasonably good correlation to the SRA curves throughout the digitized experimental response when the imperfection were in the range of 4-5%, see **Fig 3. 10** (f) and (g).

3.9.4 Layup ID 4

The beams for the anisotropic layup 15/0/-15/30 showed a slightly higher percentage error in case of the larger beam despite the fact that the buckling load was generally lower (less than

half of the buckling load of the smaller beam). Nevertheless, the analytical buckling load is on the conservative side for both beam sizes, which is practical to use in design.

As for the experimental results obtained for the larger beam, the response was in good agreement with the load-displacement curve generated from the FEA without any imperfection as there was no notional loads applied, see **Fig 3. 10** (h). Similar behavior was seen in the smaller beam as the load-displacement curve matched exactly with the curve from the non-linear response, see **Fig 3. 10** (i).

3.9.5 Layup ID 5

As for the two beams with the anisotropic layup 15/30/-45/15, the analytical prediction has a relatively sizeable error compared to the EVA. However, in both cases, the analytical load happened to be lower than the EVA loads (on the conservative side). The experimental curves for both beams match very closely to the SRA.

It is evident from **Fig. 3.** (j) and (k) that the SRA of both beam sizes starts to undergo stiffening without experiencing a real flat plateau when the initial imperfection is in the range of 4-6.5%. The larger beam seems to follow the trend while the smaller beam could not reach that level due to the off-limit deformations discussed earlier.

3.9.6 Layup ID 6

The beams of the multi-angle-ply layup 30/-30/45/-45 again reflect an excellent correspondence between the analytical and EVA loads for the larger beam while it presents a higher percentage error when comparing the same loads for the smaller beam. It is evident that both angle ply layups (Layup ID 1 and Layup ID 6) reflect a negligible percentage error for the larger beam while they show higher percentage error yet comparable for the smaller beams.

On the other hand, the experimental curve of the larger beam did not show the same flat plateau presented by the numerical solution despite the fact that both curves corresponded very well using 4% notional loads, see **Fig 3. 10** (l). As for the smaller beam size, both curves appeared to be very close at 4% notional loads while converging at the analytical buckling load, see **Fig 3. 10**(m).

It is worth mentioning that the agreement between the experimental response and the numerical behavior highly depends on the actual initial imperfection that each specimen has. While the initial imperfection depicted by the numerical Riks solution is a generalized mode 1 twisting-lateral mode at the tip of the beam, initial imperfection is expected to happen physically along the entire beam span. This makes it very hard to capture the exact curvature of the response function. Furthermore, the experimental data were digitized from hand drawn deformed sections traced by the laser dots leaving some room for minor discrepancies with an alternative higher precision process. Therefore, three trials were performed for each test to ensure the repeatability of the response.

3.10 CONCLUSIONS

In this study, experimental, numerical and analytical solutions were conducted for the purpose of direct comparisons to qualify the lateral-torsional buckling of anisotropic web-cantilever beams. During this process, four solutions were presented, namely analytical, experimental, EVA, and non-linear SRA. These results were generally in a very good agreement to each other indicating the higher reliability of the experimental tests performed. This is considered a first step to examine the behavior of web-stiffened thin shells typically used in aerospace structures. From the comparisons conducted, the following specific conclusions may be drawn:

1. The simple analytical equation developed earlier reasonably represent the actual buckling behavior as benchmarked by numerical and test results. This shows that such solutions can

contribute to the advancement of the state-of-the art computation techniques for very complex layups.

2. The test setup developed in this work proved to be effective in capturing the full non-linear response of anisotropic web cantilever beams as evident by the excellent matching with numerical solutions considering imperfect beams.
3. The EVA was also shown to be a very effective tool to arrive at economical computations to estimate lateral-torsional buckling load without the need for time-consuming non-linear analysis.
4. The numerical analysis presents a valuable and reliable means to generate results for different anisotropic layers without the need for further expensive and time-consuming experimental testing. These numerical tools may be used to conduct expensive parametric studies to optimize the anisotropic lamination for achieving various design objectives.

3.11 DATA AVAILABILITY STATEMENT

Some or all data, models, or code that support the findings of this study are available from the corresponding author upon reasonable request.

3.12 ACKNOWLEDGEMENTS

The authors would like to thank the Department of Civil Engineering at Kansas State University for supporting this research. Special thanks are due to the Research Technologists Clifford Temple and Andrew Schoenecke for helping with the testing arrangements.

3.13 APPENDIX A (SAMPLE CALCULATIONS (FOR COMPOSITE PROPERTIES)

The calculations performed for generating the mechanical properties of the tested beams are obtained using the micromechanics equations presented in Rasheed (2014). To demonstrate these calculations, a sample set of values are computed below for Layup ID 1:

3.13.1 Layup: 30/-30/30/-30

Beam Size: 485 x 51.1 mm

Given:

Modulus of Elasticity of Carbon Fiber (E_f) =234,400.000 MPa

Modulus of Elasticity of Epoxy Resin (E_m)= 2,660.260 MPa

Poisson's Ratio for Fiber (v_f) =0.170

Poisson's Ratio for Resin Matrix (v_m) =0.370

Thickness of Dry Fiber (t_f) per Layer = 0.165mm

Thickness of FRP (t_{FRP}) averaged for one layer = 0.718mm

ξ = 1

$$\text{Volume of fiber } (V_f) = \frac{\text{tf}}{\text{tFRP}} = \frac{0.165}{0.718} = 0.230$$

$$\text{Volume of Matrix } (V_m) = 1 - V_f = 1 - 0.230 = 0.770$$

$$E_1 = E_f V_f + E_m V_m = 234{,}400 \times 0.230 + 2{,}660.26 \times 0.770 = 55960.40 \text{ MPa}$$

$$E_2 = E_m \times \frac{1+\xi\eta V_f}{1-\eta V_f} = 2{,}660.26 \times \frac{1+1*0.977\times0.230}{1-0.977\times0.230} = 4202.360 \text{ MPa (Halpin} - \text{Tsai)}$$

$$v_{12} = v_f V_f + v_m V_m = 0.170 \times 0.230 + 0.370 \times 0.770 = 0.324$$

$$G_f = \frac{E_f}{2(1+v_f)} = \frac{234{,}400.000}{2(1+0.170)} = 100{,}170.940\ MPa$$

$$G_m = \frac{E_m}{2(1+v_m)} = \frac{2{,}660.26}{2(1+0.370)} = 970.897\ MPa$$

$$\eta = \frac{G_f/Gm - 1}{Gf/Gm + \xi} = \frac{1000170.940/970.897 - 1}{1000170.940/970.897 + 1} = 0.980$$

$$G_{12} = G_m \times \frac{1+\xi\eta V_f}{1-\eta V_f} = 970.897 \times \frac{1+1\times0.980\times0.230}{1-0.980\times0.230} = 1{,}535.937\ MPa$$

$$G_{23} = \frac{E_2}{2(1+v_m)} = \frac{4202.360}{2(1+0.370)} = 1{,}533.78\ MPa$$

where $E_f, E_m, V_f, V_m, v_f, v_m, G_f, G_m$ are the fiber modulus, matrix modulus, fiber volume fraction, matrix volume fraction, Poisson's ratio for fiber, Poisson's ratio for matrix, fiber shear modulus and matrix shear modulus, respectively.

3.14 APPENDIX B (SAMPLE CALCULATIONS FOR SOUTHWELL PLOT)

Below is the calculation shown for getting the buckling load using South well plot.

3.14.1 Layup: 30/30/30/30

Beam Size: 500 x 50 mm

Table 3. 5 and **Table 3. 6** represents the Load (in newton) Vs angle of twist for two trials obtained from the experimental testing of beam. Further, a scatter graph, **Fig. 3. 1**, is obtained by using the values of load and angles in table. A trendline in the graph is plotted.

Table 3. 5.Load Vs Angles (Trial 1)

Weight (in newtons)	Angles
0	0.00
2.23	0.16
4.45	1.30
5.56	3.05
6.68	5.06
7.79	10.85
8.34	15.39
8.90	23.45

Table 3. 6.Load Vs Angles (Trial 2)

Weight (in newtons)	Angles
0	0.00
2.23	0.08
4.45	2.10
5.56	3.51
6.68	5.40
7.79	9.09
8.34	14.67
8.90	20.94

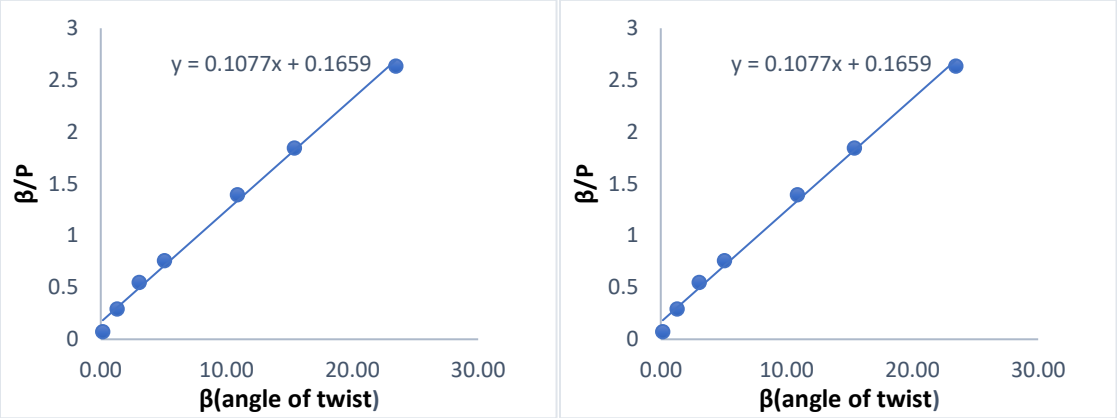

Fig. 3. 1. Load Vs Angle (Experimental Values)-Trial 1 and 2

The equation obtained from the South well plot for $\frac{\beta}{P}$ Vs β is:

$$\frac{\beta}{P} = \frac{\beta}{\text{Pcr}} + \frac{\text{a1}}{\text{Pcr}} \quad \text{.....(2)}$$

If we look at Eq. 2, this is in the standard formula of y =mx + c used for a straight line where m is slope and c is the y-intercept. Taking this into consideration, the inverse of the slope is used to calculate the Pcr.

For trial 1, slope =0.1056, Pcr = $\frac{1}{slope}$ = 9.67 N

For trial 2, slope =0.1077, Pcr = $\frac{1}{slope}$ = 9.28 N

$\text{Pcr}_{\text{final}} = \frac{9.67+9.28}{2}$ = 9.48 N

3.15 REFERENCES

Ahmadi, H. 2017. “Lateral Torsional Buckling of Anisotropic Laminated Composite Beams Subjected to Various Loading and Boundary Conditions.” *ProQuest Dissertations and Theses*. Ph.D. Ann Arbor: Kansas State University.

Anbarasu, M., and M. Kasiviswanathan. 2021. “A Simplified Design Method for Lateral–Torsional Buckling of GFRP Pultruded I-Beams.” *Arab J Sci Eng*, 46 (5): 5047–5060. https://doi.org/10.1007/s13369-020-05208-9.

Ascione, L., A. Giordano, and S. Spadea. 2011. “Lateral buckling of pultruded FRP beams.” *Composites Part B: Engineering*, 42 (4): 819–824. https://doi.org/10.1016/j.compositesb.2011.01.015.

Badjie, S., Y.-F. Li, T.-H. Hsu, and C.-H. Wu. 2012. *THREE-POINT BENDING TEST AND FINITE-ELEMENT ANALYSIS ON FRP BRIDGE DECK*.

Bank, L. C., M. Nadipelli, T. R. Gentry, and J. S. Yin. 1994. “Local Buckling of Pultruded FRP Beams: Theory and Experiment.” 417–422. ASCE.

Correia, J. R., F. A. Branco, N. M. F. Silva, D. Camotim, and N. Silvestre. 2011. “First-order, buckling and post-buckling behaviour of GFRP pultruded beams. Part 1: Experimental study.” *Computers & Structures*, Civil-Comp, 89 (21): 2052–2064. https://doi.org/10.1016/j.compstruc.2011.07.005.

Davalos, J. F., and P. Qiao. 1997a. “Analytical and experimental study of lateral and distortional buckling of FRP wide-flange beams.” *Journal of Composites for Construction*, 1 (4): 150–159. American Society of Civil Engineers.

Davalos, J. F., and P. Qiao. 1997b. “Analytical and experimental study of lateral and distortional buckling of FRP wide-flange beams.” *Journal of Composites for Construction*, 1 (4): 150–159. https://doi.org/10.1061/(ASCE)1090-0268(1997)1:4(150).

Davalos, J. F., P. Qiao, and H. A. Salim. 1997. “Flexural-torsional buckling of pultruded fiber reinforced plastic composite I-beams: experimental and analytical evaluations.” *Composite Structures*, Ninth International Conference on Composite Structures, 38 (1): 241–250. https://doi.org/10.1016/S0263-8223(97)00059-7.

EL-Fiky, A. M., Y. A. Awad, H. M. Elhegazy, M. G. Hasan, I. Abdel-Latif, A. M. Ebid, and M. A. Khalaf. 2022. “FRP Poles: A State-of-the-Art-Review of Manufacturing, Testing, and Modeling.” *Buildings*, 12 (8): 1085. MDPI.

Ghafoori, E., and M. Motavalli. 2015. “Lateral-torsional buckling of steel I-beams retrofitted by bonded and un-bonded CFRP laminates with different pre-stress levels: Experimental and numerical study.” *Construction and Building Materials*, 76: 194–206. https://doi.org/10.1016/j.conbuildmat.2014.11.070.

Halim, A. H. 2020. “Lateral Torsional Buckling of Thin-Walled Rectangular and I-Section Laminated Composite Beams with Arbitrary Layups.” *ProQuest Dissertations and Theses*. Ph.D. Ann Arbor: Kansas State University.

Hernandez, V., J. E. Roman, A. Tomas, and V. Vidal. 2006. “Lanczos methods in SLEPc.” *Polytechnic University of Valencia, Province of Valencia*.

Hollaway, L. C. 2010. “A review of the present and future utilisation of FRP composites in the civil infrastructure with reference to their important in-service properties.” *Construction and Building Materials*, Special Issue on Fracture, Acoustic Emission and NDE in Concrete (KIFA-5), 24 (12): 2419–2445. https://doi.org/10.1016/j.conbuildmat.2010.04.062.

Kasiviswanathan, M., and M. Anbarasu. 2021. “LTB - PFRP channel beams.” *Structural Engineering & Mechanics*, 77: 523–533. https://doi.org/10.12989/sem.2021.77.4.523.

Kim, N.-I., D. K. Shin, and M.-Y. Kim. 2007. “Improved flexural–torsional stability analysis of thin-walled composite beam and exact stiffness matrix.” *International Journal of Mechanical Sciences*, 49 (8): 950–969. https://doi.org/10.1016/j.ijmecsci.2007.01.007.

Laudiero, F., F. Minghini, N. Ponara, and N. Tullini. n.d. “BUCKLING RESISTANCE OF PULTRUDED FRP PROFILES UNDER PURE COMPRESSION OR UNIFORM BENDING NUMERICAL SIMULATION.” 8.

Lee, J., and S.-E. Kim. 2002. “Flexural–torsional coupled vibration of thin-walled composite beams with channel sections.” *Computers & Structures*, 80 (2): 133–144. https://doi.org/10.1016/S0045-7949(01)00171-7.

Lee, J., S.-E. Kim, and K. Hong. 2002. “Lateral buckling of I-section composite beams.” *Engineering Structures*, SEMC 2001, 24 (7): 955–964. https://doi.org/10.1016/S0141-0296(02)00016-0.

Lin, Z. M., D. Polyzois, and A. Shah. 1996. “Stability of thin-walled pultruded structural members by the finite element method.” *Thin-Walled Structures*, 24 (1): 1–18. https://doi.org/10.1016/0263-8231(95)00034-8.

Memon, B.-A., and X. Su. 2004. “Arc-length technique for nonlinear finite element analysis.” *Journal of Zhejiang University-SCIENCE A*, 5 (5): 618–628. https://doi.org/10.1631/jzus.2004.0618.

Nguyen, T. T., T. M. Chan, and J. T. Mottram. 2015. “Lateral–Torsional Buckling design for pultruded FRP beams.” *Composite Structures*, 133: 782–793. https://doi.org/10.1016/j.compstruct.2015.07.079.

Prachasaree, W., S. Limkatanyu, W. Kaewjuea, and H. V. GangaRao. 2019. “Simplified buckling-strength determination of pultruded FRP structural beams.” *Practice Periodical on Structural Design and Construction*, 24 (2): 04018036. American Society of Civil Engineers.

Qiao, P., G. Zou, and J. F. Davalos. 2003. “Flexural–torsional buckling of fiber-reinforced plastic composite cantilever I-beams.” *Composite Structures*, 60 (2): 205–217. https://doi.org/10.1016/S0263-8223(02)00304-5.

Rasheed, H. A. 2014. *Strengthening Design of Reinforced Concrete with FRP*. CRC Press.

Rasheed, H. A., H. Ahmadi, and A. Abouelleil. 2017a. “Lateral-torsional buckling of simply supported anisotropic steel-FRP rectangular beams under pure bending condition.” *Engineering Structures*, 146: 127–139. https://doi.org/10.1016/j.engstruct.2017.05.037.

Rasheed, H. A., H. Ahmadi, and A. Abouelleil. 2017b. “Lateral-torsional buckling of simply supported anisotropic steel-FRP rectangular beams under pure bending condition.” *Engineering Structures*, 146: 127–139. https://doi.org/10.1016/j.engstruct.2017.05.037.

Rasheed, H. A., H. Ahmadi, and A. H. Halim. 2020. “Stability of Thin Web Composite Cantilever Beams of Random Lamination.” *Int. J. Str. Stab. Dyn.*, 20 (13): 2041016. World Scientific Publishing Co. https://doi.org/10.1142/S0219455420410163.

Shan, L., and P. Qiao. 2005. “Flexural–torsional buckling of fiber-reinforced plastic composite open channel beams.” *Composite Structures*, 68 (2): 211–224. https://doi.org/10.1016/j.compstruct.2004.03.015.

Silva, N. M. F., D. Camotim, N. Silvestre, J. R. Correia, and F. A. Branco. 2011. “First-order, buckling and post-buckling behaviour of GFRP pultruded beams. Part 2: Numerical simulation.” *Computers & Structures*, Civil-Comp, 89 (21): 2065–2078. https://doi.org/10.1016/j.compstruc.2011.07.006.

Thumrongvut, J., and S. Seangatith. 2011. “Experimental Study on Lateral-Torsional Buckling of PFRP Cantilevered Channel Beams.” *Procedia Engineering*, The Proceedings of the Twelfth East Asia-Pacific Conference on Structural Engineering and Construction, 14: 2438–2445. https://doi.org/10.1016/j.proeng.2011.07.306.

Vo, T. P., and J. Lee. 2007. “Flexural–torsional behavior of thin-walled closed-section composite box beams.” *Engineering Structures*, 29 (8): 1774–1782. https://doi.org/10.1016/j.engstruct.2006.10.002.

Zeinali, E., A. Nazari, and H. Showkati. 2020a. “Experimental-numerical study on lateral-torsional buckling of PFRP beams under pure bending.” *Composite Structures*, 237: 111925. https://doi.org/10.1016/j.compstruct.2020.111925.

Zeinali, E., A. Nazari, and H. Showkati. 2020b. “Experimental-numerical study on lateral-torsional buckling of PFRP beams under pure bending.” *Composite Structures*, 237: 111925. https://doi.org/10.1016/j.compstruct.2020.111925.

CHAPTER 4 : PAPER 2

Validation of Lateral Torsional Buckling of Anisotropic Laminated Rectangular Thin Simple Beams under Mid-Span Concentrated Load

Garima Sharma[1], and Hayder A. Rasheed[2]

[1]M.Sc. Student, Department of Civil Engineering, Kansas State University, Manhattan, KS (garimas@ksu.edu)

[2]Professor, Department of Civil Engineering, Kansas State University, Manhattan, KS (hayder@ksu.edu)
Corresponding author

4.1 ABSTRACT

In this study, numerical evaluation and experimental testing are conducted for lateral torsional buckling of simply supported beams. Wet/hand layup was used to manufacture a total of four glass fiber-reinforced polymer beams with varying layups and length to height (L/h) ratios. To provide simply supported condition for the experimental setup, a frame of small steel tubing was designed and built. Loading was applied at the center of the beam by drilling a hole at mid-height of the beam. Two laser dots were mounted at the top and bottom of the beam to trace the angle of twist for each load increment. Non-linear numerical solution using Static Riks Analysis (SRA) was simulated to verify the experimental results. An analytical expression established in an earlier study was used to assess the critical buckling load.

4.2 INTRODUCTION

In the field of aerospace, marine, mechanical and civil engineering, thin-walled beam structures are major base components. During recent times, fiber-reinforced polymers (FRP) have been replacing traditional materials in several of these structures. The rising popularity could be attributed to some of its superior characteristics like high strength-to-weight ratio, high stiffness-to-weight ratio, and corrosion resistance. The most distinguished feature of FRP composites is the ability to tailor the material for each particular application. Despite having significant advantages, due to their low stiffness and slenderness, problems of excessive

deformation and instability are major limitations in the wider acceptance for structural engineering applications. Before FRP structures approach material failure, the dominant design limit state for these structures usually include consideration of stability and deformation. As a result, the appropriate establishment of such criteria is a prerequisite for the practical use of FRP in engineering applications.

Many researchers have focused on studying the lateral torsional buckling of composite beams.

Lin et al. 1996 studied stability of thin-walled pultruded structural members by the finite element method. Davalos and Qiao developed an analytical equation for lateral and distortional buckling of FRP wide flange beams which was verified with experimental testing.

Lee et al. 2002 studied lateral buckling of I-section composite beams. Based on classical lamination theory, a general analytical model subjected to various types of loadings was developed. The model considers the material coupling for arbitrary laminate stacking sequence configuration, effect of the location of applied loading and various boundary conditions. To predict critical loads and corresponding buckling modes, displacement-controlled finite element analysis is analyzed. Based on the numerical and analytical results, the study concludes that lateral buckling capacity of beams with transverse loads are affected by the location of applied load as well as the fiber orientation, for the beam under pure bending with off-axis fiber orientation, orthotropic closed-form solution is not appropriate for predicting lateral buckling loads due to the existence of coupling stiffness.

Laudiero et al. 2012 simulated a numerical approach for the buckling resistance of pultruded FRP profiles under pure compression and uniform bending in two parts. The first section used non-linear finite element analysis to determine the buckling mode interaction in wide flange columns under pure compression while accounting for imperfections. The numerical results indicated that

the imperfection amplitude played a crucial role making the columns unsafe. In the second part, a similar approach was used for beams with uniform bending. Finally, an expression for the rotational spring stiffness of the web-flange junction was proposed, yielding more accurate results for local buckling.

Badjie et al. 2012 studied the mechanical behavior and failure mechanisms of a Glass Fiber Reinforced Plastic (GFRP) composite bridge deck using three-point bending experiments. For this study, three distinct GFRP composite bridge panel types were examined. One is the prototype panel, an epoxy mortar-filled GFRP panel is the second one, and the third is an epoxy mortar-filled GFRP panel wrapped with carbon fiber. The finite element analysis revealed a 12.8% inaccuracy corresponding to the experimental results.

Lateral torsional buckling (LTB) design for pultruded FRP (PFRP) beams was studied by Nguyen et al. 2015.A design procedure was proposed based on Eurocode for the LTB of the beams. The test population for calibration had 114 LTB buckling resistances using four PFRP section sizes of I and channel shapes. Test results from the 114 beams were used to generate a single LTB formula considering the partial factor of resistance. An imperfection factor of 0.34 and partial factor of safety of 1.3 was shown to be appropriate for calculation of the LTB moment of resistance.

Prachasaree et al. 2019 proposed a simplified buckling strength equation for lateral torsional buckling and local buckling strengths of FRPs structural members. The proposed equation was compared to a pre-standard equation and experimental data gathered from previous research works. When compared to experimental data, the results for lateral torsional buckling were conservative. Furthermore, when compared to buckling strength based on pre-standard equations, LTB was directly proportional to its unbraced length. The proposed equation

demonstrated 15% average percentage difference with the experimental data for local buckling strength. The authors suggest that that results were accurate and reliable for easier calculations.

Zeinali et al. 2020 investigated the lateral-torsional buckling of pultruded fiber reinforced beams under pure bending using a combined experimental and numerical approach. The studies were carried out on eleven beams with varied height to span ratios and two types of I shaped profiles. For the analytical technique, the Eurocode 3 equation was used for computations. Finally, finite element analysis was used to validate the analytical and experimental results. The experimental findings were consistent with the numerical and analytical results.

Ahmadi and Rasheed 2018 derived an analytical expression for the Lateral Torsional Buckling of simply supported beams for fiber reinforced polymer under varying layups. In this study, an experimental and finite element analysis is performed to benchmark the analytical formulation.

4.3 ASSUMPTIONS

The following assumptions were made in the analytical treatment established earlier:

1) The material is generally anisotropic laminated composite with elastic properties using thin plate classical lamination theory.
2) The kinematics assumes twisting angle to be constant across the height of the beam.
3) The strain-displacement relationship is assumed to be linear.
4) The equilibrium equation is linearized for buckling analysis.
5) The non-linear terms from the loading are retained in the governing differential equation.

The following assumptions are made in the numerical treatment addressed herein:

6) The material is generally anisotropic laminated composite with elastic properties using moderately thick shell elements.

7) The kinematics captures the actual variation of the twisting angle across the height of the beam.
8) The strain-displacement relationships are assumed to be non-linear within Riks Analysis.
9) The equilibrium equations are linearized for Eigen Value Analysis while they are fully non-linear within Riks Analysis.
10) The imperfections are treated using notional loads.

Assumption 1 is proven to be accurate experimentally since the beam goes to its original undeformed configuration after load removal indicating no induced and sustained damage.

4.4 COMPOSITE BEAM FABRICATION PROCESS

The composite beams used in the experimental study were prepared with wet/hand layup process at the Department of Civil Engineering at Kansas State University. For beam preparation, two materials were required: Glass fiber (V Wrap E G50) and matrix (V-Wrap 770 2022). Since the glass fibers attained from the manufacturer were unidirectional, the fibers were cut at desired angles. The four dry layers of the beam were cut to size and laminated using the same process. Hereafter, two-component resin was prepared to saturate the beam.

To hold the initial layer of fiber, a layer of wax paper was applied first, followed by a layer of the binding matrix. Subsequently, the second layer of the fiber was placed with a coat of epoxy on top of it. To create a four-layered composite beam, the method was repeated for each layer. The manufactured composite beams were then left at room temperature for seven days in the lab for curing, **see Fig. 4.1.** The beams were then cut to their proper dimensions, **see Table 4.1.** Four holes were bored on either end of the beams to hold plates at the ends required to achieve the suppression of section twisting at the simply support condition.

Table 4.1. Beam Designations and Dimensions

Layup ID	Dimension (mm) Length x Height	Thickness(mm)	Layup sequence
1	500 x 50	3.750	15/0/-15/30
2	500 x 50	4.543	15/30/-45/15
3	500 x50	4.230	30/-30/45/-45
4	500 x 25	4.530	30/-40/50/-60

Fig. 4.1. Beams left for curing at room temperature

4.5 MATERIAL CHARACTERIZATION

The glass fiber used to manufacture the present composite beams is V-Wrap EG-50 having the mechanical properties given in **Table 4.1.**. A two-component epoxy resin named V-wrap 770, **Table 4.2**., was used to saturate the fiber by following the wet layup manufacturing process. By using the properties of the dry fiber and the resin as well as the principles of composite micromechanics, the cured laminate properties were computed as per Rasheed (2014).The results are listed in **Table 4.3.**

Table 4.2.V-Wrap E-G50 fiber (dry) and V-Wrap 770 epoxy resin mechanical properties

Property	Value
V-Wrap EG50	
Primary fiber direction	0 degree (unidirectional)
Weight per square yard	915 g/m^2
Tensile strength	3,275 MPa
Tensile modulus	79,970 MPa
Thickness	1.016 mm
Elongation	2.13%
V-Wrap 770 Epoxy adhesive	
Flexural Modulus	2,620 MPa
Poisson's ratio	0.0315

Table 4.3. Cured laminate properties recovered from micromechanics relationships.

Layup ID	Dimensions (mm)	E_1 (MPa)	E_2 (MPa)	v_{12}	G_{12} (MPa)	G_{23} (MPa)
1	500 x 50	32281.09	8062.73	.314	2967.42	2942.60
2	500 x 50	27342.80	7080.18	.324	2601.27	2584.00
3	500 x50	29071.90	7405.46	.320	2722.37	2702.72
4	500 x 25	27411.51	7092.75	.324	2605.94	2588.59

4.6 EXPERIMENTAL SETUP

For the experimental setup, a frame was fabricated using steel tubing with plexi-glass connected to one end on which Engineering Paper was attached, **see Fig 4.2.** The frame was designed to provide flexibility in achieving the boundary conditions. For instance, one end of the beam was secured with four screws and fastened to a plate that is allowed to only rotate. This fixture resembles a pin support as depicted in **Fig 4.3.** In addition, the entire edge was fabricated in a way that allows adjusting the spacing between both ends so that it can accommodate varying beam lengths.

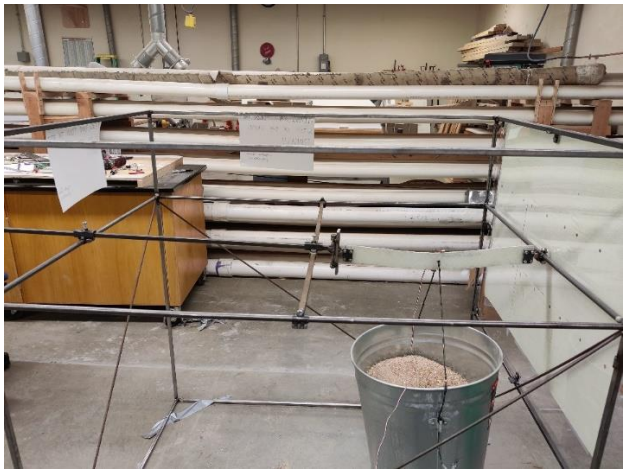

Fig. 4.2. Frame setup with attached plexi-glass

Fig. 4. 3. Beams screwed for boundary condition

Fig. 4. 4. Laser dots mounted for deformation

The beams were tested in simply supported condition and the loading was done at the center of the beam. A hole was drilled at the mid-section of the beam in which an annular steel bush was inserted to prevent the beam from any damage caused due to stress concentration while loading. **Fig. 4.4.** shows two laser dots positioned at top and bottom of the beam to trace the deformation of the beam. Steel binding wires were passed through the hole that were connected to the two sides of a bucket. The load is then applied by adding

weighted amount of sands into the bucket which results in buckling of the beams, **see Fig.4.5.** For each loading step, the deformation is recorded with the projected laser lights on the Engineering paper, **see Fig. 4.6**. The outcomes of the traced markings were digitized in order to get the experimental curves using a software called “web plot digitizer”.

Fig. 4.5. Beam in buckling configuration

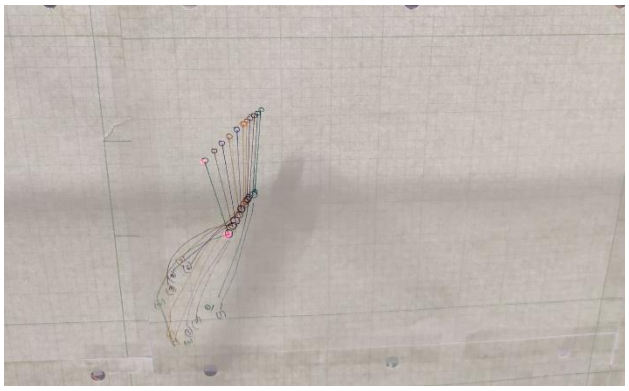

Fig. 4.6.Deformation lines being traced with projected laser light

4.7 NUMERICAL ANALYSIS

Numerical analysis was carried out in two consecutive simulation approaches with the program Abaqus. The first approach uses Eigen Value Analysis (EVA) to determine the projected buckling load for the layup, dimensions and material parameters involved, which is compared to the buckling load derived through analytical formulation. Following this technique, non-linear Static Riks Analysis (SRA) was invoked to capture the full non-linear behavior of the beam.

4.7.1 Eigen Value Analysis (EVA)

Mechanical properties of the cured laminates were input into the software. The beams in the model were created using 3D planar thick shell elements (S8R). After the beam with its proper dimensions was generated, the stacking sequence was input in the software using the composite layup. Following the composite layup process, the material properties in different directions were assigned to the beam. To obtain the center of the beam for load application, the partitioning tool in Abaqus was used. A specific load was applied at the center of the beam. For the boundary condition, a total of six nodes were specified. Four nodes at the extreme corner of the beam that were restrained in the z-axis displacement to prevent section twisting at the simple support. The node at the mid-height of one edge was pinned and a roller was used at the mid-height of the other edge, see Error! Reference source not found.**.** Before the analysis, the beam was meshed with standard quadratic quadrilateral shell element type of S8R (8- node doubly curved thick shell element with reduced integration) with a mesh size of 1mm along the beam axis. The value obtained from Abaqus for the first mode was multiplied by the applied load amount to get the actual buckling load.

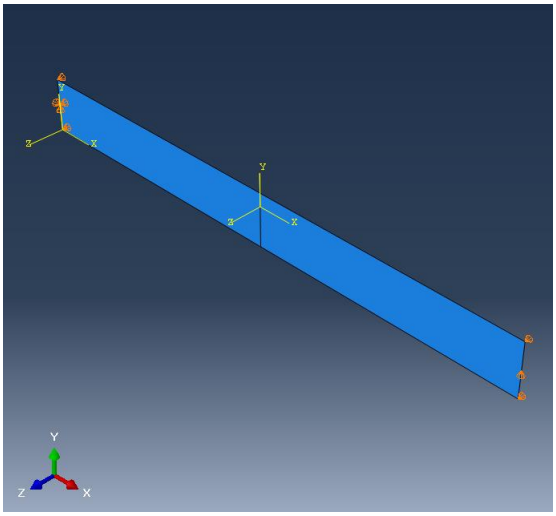

Fig. 4. 7.Boundary conditions applied at respective nodes

4.7.2 Static Riks Analysis (EVA)

Static Riks Analysis is performed to capture the non-linear behavior of the beams. This method uses arc length technique in which a portion of load is initially applied as a load step to determine the load-displacement values for normalizing subsequent steps.

The buckling load obtained from the Eigen value analysis was used to define the target maximum load which is used by the arc length solver to determine the intermediate load steps based on defined increments. Different notional loads were applied to produce an equivalent initial imperfection in the angle of twist. These notional loads are defined as small percentages of the actual applied vertical mid-span force. The direction of the notional loads was determined by the buckling behavior observed in EVA, see **Error! Reference source not found.-Error! Reference source not found.**. To account for the fixity of the boundary conditions observed during the experimental results, a spring constant was introduced in the middle nodes at both ends.

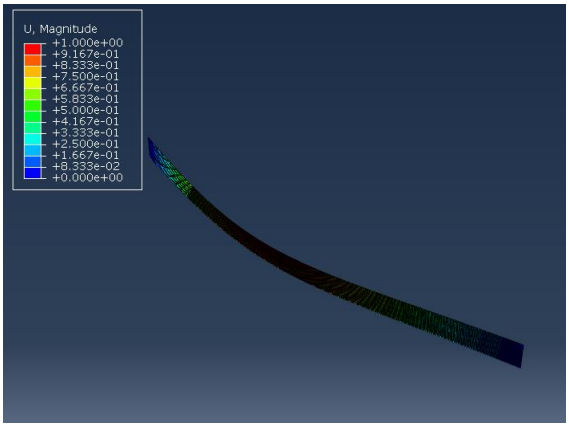

Fig. 4. 8. Beam in deformation during numerical analysis

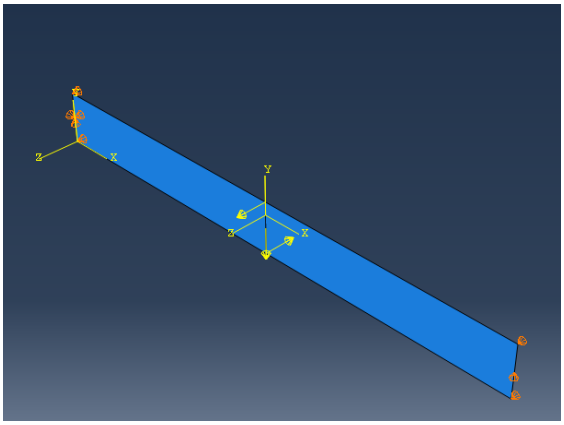

Fig. 4. 9. Imperfections accounted with notional loads

4.8 ANALYTICAL FORMULATION

Ahmadi and Rasheed 2018 established a solution based on classical lamination theory for making analytical predictions. In terms of the lateral, torsional and coupling stiffness coefficients of the composite, a closed form buckling expression was developed. These coefficients were obtained through dimensional reduction by static condensation of the general 6 x 6 constitutive matrix mapped into an effective 2 x 2 coupled weak axis bending-twisting relationship. The resulting two coupled stability differential equations were manipulated to yield a single governing differential equation in terms of the twisting angle. Mathematica was used to solve the differential equation with variable coefficients and suitable boundary conditions. To generate the semi-analytical solution, the resultant solution was found to correlate with the effective lateral-flexure, torsional, and coupling stiffness. The entire analytical formulation was presented in detail in an earlier article by Ahmadi and Rasheed 2018. The critical buckling load can be calculated from the formula given below in Eq. (1).

$$P_{Cr} = \frac{16.94h}{L^2}\sqrt{4[D_Y D_T - {D_{YT}}^2]} \qquad \text{Eq. (2)}$$

where D_Y is the composite effective lateral stiffness coefficient, D_T is the composite effective twisting stiffness coefficient and D_{YT} is the composite effective lateral-twisting coupling coefficient.

4.9 RESULTS AND DISCUSSIONS

Four simply supported beams with mid height loading were tested at the Department of Civil Engineering at Kansas State University. The nominal length dimensions for the tested beams were 500mm with nominal height dimension of 50 mm and 25 mm corresponding to (l/h) ratio of 10 and 20 respectively.

` **Error! Reference source not found.** also presents a comparison of the analytical prediction, Eigen value extraction and projected experimental buckling loads for all the beams constructed. The analytical critical buckling load was obtained for the simply supported boundary condition. However, there seems to be presence of certain amount of rigidity in the supports because of the application of screws to hold the beam in position, see **Fig 4.3.**.

Table 4. 4.Analytical, numerical and apparent experimental buckling loads for all beams.

Layup ID	Dimension (mm)	Layup Sequence	Analytical buckling load (N)	Eigen value (N)	% Error	Maximum experimental load (N)
1	500 x 50	15/0/-15/30	294.42	288.56	2.03	289.25
2	500 x 50	15/30/-45/15	453.79	431.16	5.25	511.75
3	500 x50	30/-30/45/-45	369.40	354.31	4.26	400.5
4	500 x 25	30/-40/50/-60	193.40	175.61	10.13	244.75

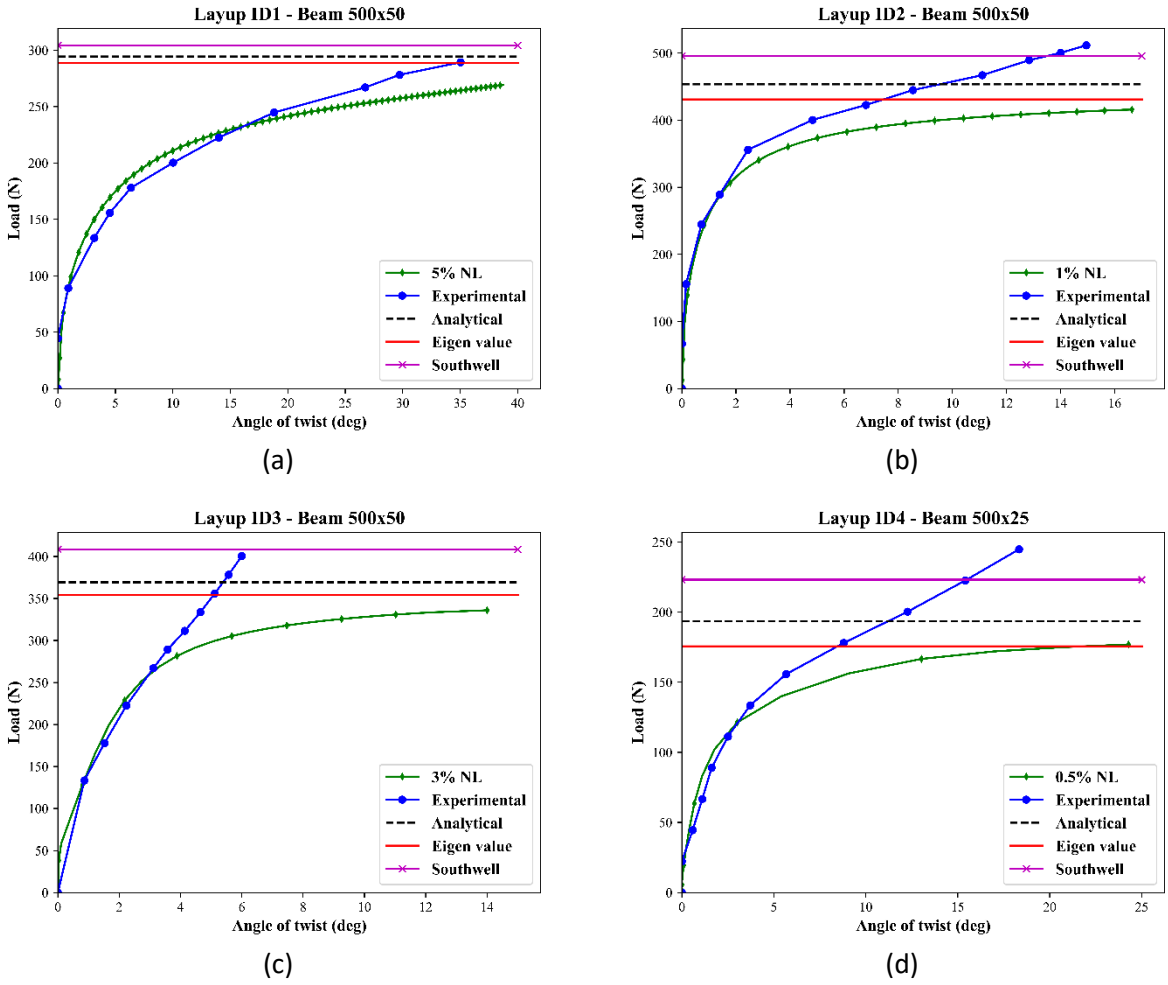

Fig. 4. 10. Load Vs Angle of twist for all beams examined

4.9.1 Layup ID 1: 15/0/-15/30

For the anisotropic layup 15/0/-15/30, the critical buckling load obtained from the analytical formulation is in good correspondance with the buckling load obtained from EVA. Furthermore, the values for the load obtained for the projected experimental buckling from the Southwell plot is in close agreement with the other two methods, **see fig 4.10.(a)**

As for the experimental results obtained for the beam, the response was in good agreement with the load-displacement curve generated by Finite Element Analysis (FEA) when the imperfection was 0.5%.

4.9.2 Layup ID 2: 15/ 30/-45/15

For the beam with Layup 15/30/-45/15, there is sizeable discrepancy between the buckling load obtained from the south well plot compared to EVA and analytical formulation. Despite the discrepancy, the analytical results happen to be on the conservative side than the Southwell value, **see fig 4.10.(b)**

It is evident from **fig 4. 10.(b)** that the SRA results converge at a lower load experiencing a flat plateau which cannot be seen on the experimental response. The load-displacement curve for the experimental and numerical response match well with the application of 1% notional load in the initial loading range.

4.9.3 Layup ID 3: 30/-30/45/-45

The beam for the multi-layup 30/-30/45/-45 depicts close value results for EVA and analytical methods. However, the results obtained from the experiments for the buckling load is higher as represented by the Southwell calculation. This may be attributed to the physical rigidity experienced by the test specimen at the boundary conditions.

Again, **fig 4.10.(c)** shows with the application of 3% notional load in the direction of buckling observed in EVA, the numerical response deviates from the experimental response while still being in correspondence in the initial loading zone.

4.10 Layup ID 4: 30/-40/50/-60

The beam with stacking sequence 30/-40/50/-60 illustrate small discrepancy for the buckling load obtained between the three methods. The EVA seems to be on the lower bound than analytical and Southwell calculation.

A similar trend can be seen in **fig 4.10.(d)** for the non-linear behavior with the values from the experimental and numerical results matching in the initial loading zone while diverging as it approaches the buckling loading zone.

4.11 CONCLUSIONS

In this study, experimental, numerical and analytical solutions were conducted for the purpose of direct comparisons to qualify the lateral-torsional buckling of simply supported beams. During this process, four solutions were presented, namely analytical, experimental, EVA, and non-linear SRA. From the comparisons conducted, the following specific conclusions may be drawn:

1. The numerical response obtained matched well with the experimental results in the initial loading zone. The discrepancy in the buckling loading zone can be explained by the presence of certain rigidity in the boundary conditions during the experiments.
2. The analytical results were on the lower bound in comparison to the Southwell computations.
3. Improved correspondence of the results may be possible by numerically modeling the end plates used to prevent twisting of end sections as well as slightly reduced clear span values in the analytical solution.

REFERENCES

Ahmadi, H., and H. A. Rasheed. 2018. “Lateral torsional buckling of anisotropic laminated thin-walled simply supported beams subjected to mid-span concentrated load.” *Compos. Struct.*, 185: 348–361. https://doi.org/10.1016/j.compstruct.2017.11.027.

Badjie, S., Y.-F. Li, T.-H. Hsu, and C.-H. Wu. 2012. *THREE-POINT BENDING TEST AND FINITE-ELEMENT ANALYSIS ON FRP BRIDGE DECK*.

Davalos, J. F., and P. Qiao. 1997. “Analytical and experimental study of lateral and distortional buckling of FRP wide-flange beams.” *J. Compos. Constr.*, 1 (4): 150–159. https://doi.org/10.1061/(ASCE)1090-0268(1997)1:4(150).

Laudiero, F., F. Minghini, N. Ponara, and N. Tullini. n.d. “BUCKLING RESISTANCE OF PULTRUDED FRP PROFILES UNDER PURE COMPRESSION OR UNIFORM BENDING NUMERICAL SIMULATION.” 8.

Lee, J., S.-E. Kim, and K. Hong. 2002. “Lateral buckling of I-section composite beams.” *Eng. Struct.*, SEMC 2001, 24 (7): 955–964. https://doi.org/10.1016/S0141-0296(02)00016-0.

Lin, Z. M., D. Polyzois, and A. Shah. 1996. “Stability of thin-walled pultruded structural members by the finite element method.” *Thin-Walled Struct.*, 24 (1): 1–18. https://doi.org/10.1016/0263-8231(95)00034-8.

Nguyen, T. T., T. M. Chan, and J. T. Mottram. 2015. “Lateral–Torsional Buckling design for pultruded FRP beams.” *Compos. Struct.*, 133: 782–793. https://doi.org/10.1016/j.compstruct.2015.07.079.

Prachasaree, W., S. Limkatanyu, W. Kaewjuea, and H. V. GangaRao. 2019. “Simplified buckling-strength determination of pultruded FRP structural beams.” *Pract. Period. Struct. Des. Constr.*, 24 (2): 04018036. American Society of Civil Engineers.

Rasheed, H. A., H. Ahmadi, and A. Abouelleil. 2017. “Lateral-torsional buckling of simply supported anisotropic steel-FRP rectangular beams under pure bending condition.” *Eng. Struct.*, 146: 127–139. https://doi.org/10.1016/j.engstruct.2017.05.037.

Zeinali, E., A. Nazari, and H. Showkati. 2020. “Experimental-numerical study on lateral-torsional buckling of PFRP beams under pure bending.” *Compos. Struct.*, 237: 111925. https://doi.org/10.1016/j.compstruct.2020.111925.

CHAPTER 5 : CONCLUSIONS

Lateral torsional buckling of thin-walled cantilever and simply supported beams is studied. In this study, experimental testing and numerical iterations are carried out to benchmark the analytical solution developed earlier.

Two different analytical equations developed earlier using closed form solution was used to find the critical buckling load of web-cantilever carbon fiber reinforced polymer beams and simply supported glass fiber reinforced polymer beams. A total of twelve beams for cantilever configuration and four beams for simply supported boundary conditions with varying stacking sequence were tested experimentally to get the load-displacement curve. Static Riks Analysis (SRA) was used to predict the non-linear behavior of the beams. The experimental curves generated were verified with the numerical outcomes. The resulting solutions showed very good agreement between the three approaches, i.e. Analytical, Experimental and Numerical indicating that the investigation yielded accurate findings in case of the cantilever beams. However, the discrepancy observed in the non-linear and experimental curves in case of simply supported beams could be ascribed to the presence of rigidity in the beams boundary condition. Further refinements will be made to improve the correspondence of the numerical and experimental curves by depicting the physical rigidity of the boundary condition in the model as much as possible.

It is recommended to extend this study to examine various l/h ratios in the tested beams coupled with varying anisotropic stacking sequences to widen the acceptance of the present validation process.